Table 2. Sensitivity, specificity, PPV, and NPV of CTV-Gd and CTV-T_2

Protocol	Sensitivity*	Specificity	PPV	NPV
CTV-Gd Mean (SD) (%)	**28.6 (5.2)**	99.4 (1.0)	73.6 (29.7)	95.1 (4.2)
CTV-Gd (2 mm) Mean (SD) (%)	**44.3 (30.1)**	98.8 (1.6)	68.0 (27.2)	95.9 (4.0)
CTV-Gd (5 mm) Mean (SD) (%)	**55.6 (30.2)**	**97.8 (2.3)**	**59.8 (24.5)**	**96.5 (3.7)**
CTV-Gd (10 mm) Mean (SD) (%)	**72.0 (27.9)**	**94.8 (4.2)**	**44.3 (19.6)**	**97.4 (3.3)**
CTV-Gd (20 mm) Mean (SD) (%)	**86.4 (21.5)**	**84.2 (8.7)**	**24.7 (13.5)**	**98.4 (2.5)**
CTV-T2 Mean (SD) (%)	61.1 (25.5)	97.2 (2.8)	**58.0 (26.8)**	**97.1 (2.8)**
CTV-T2 (2 mm) Mean (SD) (%)	72.4 (24.2)	95.1 (4.2)	**48.9 (24.7)**	**98.0 (2.5)**
CTV-T2 (5 mm) Mean (SD) (%)	81.9 (21.5)	**92.2 (5.7)**	**40.4 (21.8)**	98.4 (2.2)
CTV-T2 (10 mm) Mean (SD) (%)	89.4 (15.1)	**85.5 (8.8)**	**28.5 (16.6)**	**98.9 (1.7)**
CTV-T2 (20 mm) Mean (SD) (%)	96.4 (7.0)	**68.3 (13.4)**	**15.9 (9.6)**	**99.6 (1.3)**

Abbreviations: NPV = negative predictive value; PPV = positive predictive value; SD = standard deviation.

* Values in boldface type indicate $p < 0.05$ using Tukey-type multiple comparisons.

were grouped according to the RTOG recursive partitioning analysis (RPA) class (21). Most patients were put into RPA class IV ($n = 19$), and smaller numbers were in classes VI ($n = 8$), III ($n = 3$), and V ($n = 8$).

Table 2 shows sensitivity, specificity, PPV, and NPV for CTV-Gd (x mm) and CTV-T_2 (x mm). The sensitivity of CTV-Gd (20 mm) (86.4%) was significantly higher than that of the other CTV-Gd ($x = 0, 2, 5, 10$ mm). The specificity of CTV-Gd ($x = 0, 2, 5$ mm) was significantly higher than that of the other CTV-Gd ($x = 10, 20$ mm). The PPV of CTV-Gd ($x = 0, 2$ mm) was significantly higher than that of the other CTV-Gd ($x = 5, 10, 20$ mm). The NPV of CTV-Gd ($x = 20$ mm) was significantly higher than that of the other CTV-Gd ($x = 0, 2, 5, 10$ mm). The sensitivity of CTV-T_2 (20 mm) (96.4%) was significantly higher than that of the other CTV-T_2 ($x = 0, 2, 5$ mm). The specificity of CTV-T_2 ($x = 0$ mm) was significantly higher than that of the other CTV-T_2 ($x = 5, 10, 20$ mm). The PPV of CTV-T_2 ($x = 0$ mm) was significantly higher than that of the other CTV-T_2 ($x = 0, 2, 5, 10, 20$ mm). The NPV of CTV-T_2 ($x = 20$ mm) was significantly higher than that of the other CTV-T_2 ($x = 0, 2, 5, 10$ mm).

Figure 2 shows the sensitivity and specificity values of CTV-Gd ($x = 0, 2, 5, 10, 20$ mm) and that of CTV-T_2 ($x = 0, 2, 5, 10, 20$ mm). The highest sensitivity and lowest specificity values were shown by CTV-T_2 ($x = 20$ mm). The lowest sensitivity and highest specificity values were shown by CTV-Gd ($x = 0$ mm). Table 3 compares our results with those reported by Jansen *et al.* (19), correlating histopathologic observations and use of CT or MR images. Hochberg *et al.* (22) reported 29/35 (82.9%) tumor cells were within 2 cm

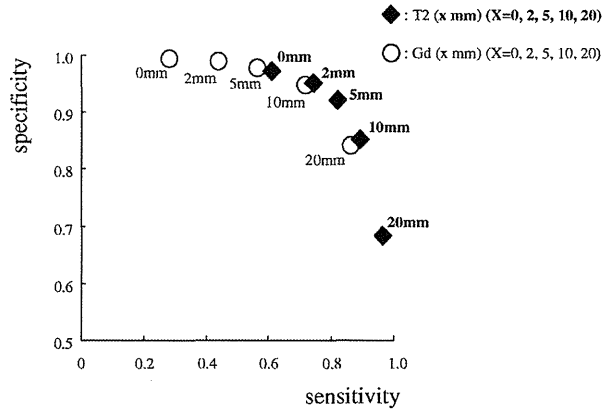

Fig. 2. Scatter plot of T_2-weighted MRI (x mm) (where $x = 0, 2, 5, 10, 20$ mm) and Gd (x mm) ($x = 0, 2, 5, 10, 20$ mm) with respect to sensitivity and specificity, respectively.

of the tumor mass on CT, and in our study, 86.4% of tumor cells were within 2 cm of the tumor mass on MRI. Burger *et al.* (23) reported 5/5 (100%) tumor cells were within the necrotic area plus 3 cm. Although we do not discuss CTV-Gd plus 3 cm in our study, we expect results were nearer to 100% (more than CTV-Gd [20 mm]). Halperin *et al.* (24) reported 9/11 (81.8%) tumor cells were beyond the enhancement area on CT, and 11/11 (100%) tumor cells were within the edema area; in our study, 71.4% of tumor cells were beyond the Gd enhancement area, and although we do not discuss CTV-T_2 plus 3 cm, we expect results were almost 100% (more than CTV-T_2 [20mm]). Because other studies (25–27) included patients with not only GBM but also anaplastic astrocytoma, results differ slightly from our data.

DISCUSSION

Brain tumor tissue can be visualized with MRI and CT because of the increased water content (edema) compared with normal brain tissue and because of disruption of the blood–brain barrier, and the tumor tissue is visualized as contrast enhancement. However, neither contrast enhancement nor edema is always a real measure of the extent of tumor for gliomas. Tumor cells have been detected beyond the margins of contrast enhancement, in the surrounding edema and even in adjacent brain tissue that appears normal. After neurosurgery or radiotherapy, blood–brain barrier disturbances and edema can also be treatment-related, and they cannot be differentiated from persistent tumor on CT or MRI (25, 28–31). Therefore, after the introduction of CT and MRI as planning methods for irradiation of postoperative GBM, many investigators have tried to define the optimal treatment volume. However, there are many studies that report where tumor exists outside of the edema and the enhanced area of CT and MRI, and this topic is still a matter of heated debate.

Comparative analyses among CT, MRI, and [^{11}C]MET-PET and stereotactic biopsies suggest that [^{11}C]MET-PET

Table 3. Comparison of correlations of histopathologic observations and use of CT or MR images

Institution (ref)	No. of patients	No. of GBM tumor cells/total no. of AA	CT or MRI	Pathologic findings	Results	This results
MGH (22)	35	Not specified	CT	Tumor cells within 2 cm of tumor mass on CT	29/35 (82.9%)	86.4%
Duke (23)	5	5/0	CT	Tumor cells within Necrotic area plus 3 cm	5/5 (100%)	86.4% <
Duke (24)	11	15/0	CT	Tumor cells go beyond enhancement	9/11 (81.8%)	71.4%
				Tumor cells within Edema plus 3 cm	11/11 (100%)	96.4% <
Mayo (25)	40	8/7	CT/MRI	Tumor cells within hypodense (CT), T_2 high (MRI)	15/16 (93.8%)	61.1%
				Tumor cells within isodense (CT), T_2 high (MRI)	14/14 (100%)	
Brain R.I. Niigata (26)	18	6/12	CT/MRI	Tumor cells go beyond T2 high (MRI)	4/18 (22.2%)	38.9%
Barrow (27)	5	3/2	MRI	Tumor cells within T2 high (MRI)	5/5 (100%)	61.1%

Abbreviations: MGH = Massachusetts General Hospital, MA; Duke = Duke University, NC; Mayo = Mayo Clinic, MN; Brain R.I. Niigata = Brain Research Institute, Niigata, Japan; Barrow = Barrow Neurological Institute; AZ GBM = glioblastoma multiforme; AA = anaplastic astrocytoma.

has greater accuracy for defining the extent of glioma than CT and MRI (10, 13, 18). The integration of [^{11}C]MET-PET into radio-oncologic treatment planning has provided encouraging results because [^{11}C]MET-PET is highly sensitive in the context of brain tumor tissue. In the present study, the biological target volume using [^{11}C]MET-PET helped to describe tumor morphology (GTV) with greater accuracy than traditional radiologic modalities (such as MRI) alone (10, 18, 32). The results of this study demonstrate that [^{11}C]MET-PET improves visualization of the extent of GBM (Fig. 3).

Table 3 compares the present results with those reported by Jansen et al. (19), correlating histopathologic observations and CT/MR images. Although some studies report different results (22–27), for example, tumor cells exist within the tumor plus α and edema plus β, those results almost corresponded to our results, for which [^{11}C]MET-PET findings served as the gold standard in this study. In a word, it is thought that our results are valid by near correspondence to histopathologic observations.

Methionine is a natural amino acid that is briskly taken up by glioma cells, with only a low uptake in normal cerebral tissue. The uptake is mediated mainly by the L-type amino acid transport system. Methionine may be used for protein synthesis or is converted to *S*-adenosylmethionine, which is the primary methyl donor for transmethylation reactions and a precursor of polyamide synthesis. A smaller part of MET is metabolized by decarboxylation. However, several experiments have suggested that during [^{11}C]MET-PET studies, the tumor uptake of [^{11}C]MET mainly reflects increased amino acid transport (12, 13, 20). Therefore, [^{11}C]MET-PET does not directly receive the influence of the operation easily, because of the high possibility of showing the tumor localization. It is thought that an

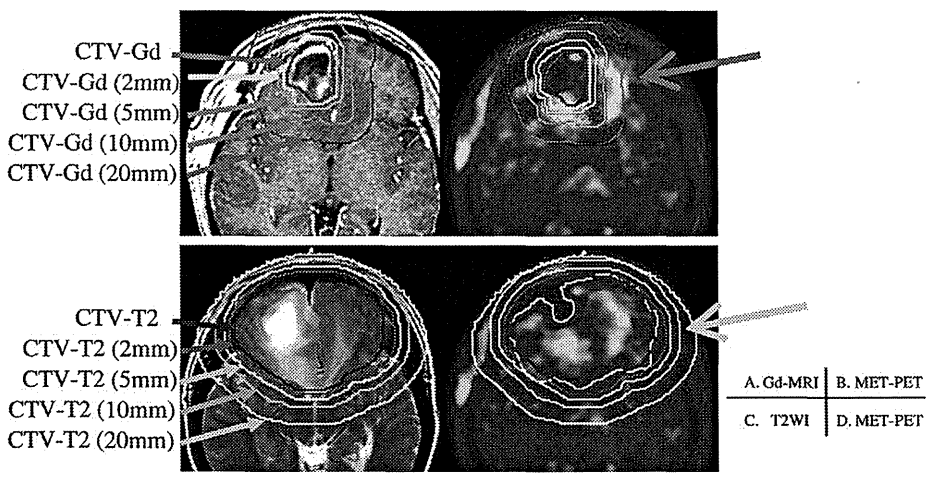

Fig. 3. Example of Gd-enhanced MRI scans illustrating (A, upper left) CTV-Gd (x mm) as x mm (x = 0-, 2-, 5-, 10-, and 20-mm) margin outside the CTV-Gd, respectively. And these lines were superimposed onto [^{11}C]MET-PET images (B, upper right) in the same patient. (C, lower left) Example of T_2-weighted MRI scans illustrating CTV-T2 (x mm) as x mm (x = 0-, 2-, 5-, 10-, 20-mm) margin outside the CTV-T2, respectively. These lines were superimposed onto [^{11}C]MET-PET images (D, lower right) in the same patient. The area is too small (red arrow) to contain CTV-PET by CTV-Gd (20mm) line (B). The area is too large (green arrow) to minimize the radiation exposure to the normal brain tissue (D).

excellent agreement was seen this time. We believe the results of this study demonstrate that [^{11}C]MET-PET has a substantial impact on visualizing the extent of GBM.

To optimize tumor control and prevent local failure, it is necessary to raise the sensitivity of the defined target as much as possible. In our study, when we used a 2-cm margin to the CTV-Gd, the sensitivity was 86%, so this was not adequate. When a 2-cm margin to the CTV-T_2 was used, the sensitivity was 96%, so a 2-cm margin to the CTV-T_2 is best to optimize tumor control and to prevent local failure. Therefore, it is necessary to use at least a 2-cm margin to the CTV-T_2 for the initial target planning of radiation therapy. However, if dose escalation to the 2-cm margin is performed in the CTV-T_2, because the specificity is 68%—and this is low—then the dose of radiation to the normal tissue increases and the possibility of radiation damage to normal tissue is expected to rise. [^{11}C]MET-PET cannot be used to target the dose escalation, and it is necessary to set an appropriate margin to the CTV-Gd or CTV-T_2 in each case. Therefore, there is a limit to the optimal margin when using Gd-MRI and T_2-MRI.

CONCLUSION

It is necessary to use a margin of at least 2 cm in T_2-MRI for the initial target planning of radiation therapy. However, in radiation planning for postoperative patients with GBM, the CTV-Gd and CTV-T_2 margins differed considerably from that of CTV- [^{11}C]MET-PET. There is a limit to the optimal margin in this setting of the Gd-MRI and T_2-MRI. Thus, rather than using Gd-MRI and T_2-MRI, [^{11}C]MET-PET has promising potential for precisely delineating target volumes in planning radiation therapy for postoperative patients with GBM.

REFERENCES

1. Stupp R, Mason WP, van den Bent MJ, *et al.* Radiotherapy plus concomitant and adjuvant-temozolomide for glioblastoma. *N Engl J Med* 2005;352:987–996.
2. Nelson DF, Diener-West M, Horton J, *et al.* Combined modality approach to treatment of malignant gliomas (re-evaluation of RTOG7401/ECOG 1374 with long-term follow-up. A joint study of the Radiation Therapy Oncology Group and the Eastern Cooperative Oncology Group). *Natl Cancer Inst Monogr* 1988;6:279–284.
3. Stupp R, Dietrich PY, Ostermann KS, *et al.* Promising survival for patients with newly diagnosed glioblastoma multiforme treated with concomitant radiation plus temozolomide followed by adjuvant temozolomide. *J Clin Oncol* 2002;20:1375–1382.
4. Chan JL, Lee SW, Fraass BA, *et al.* Survival and failure patterns of high-grade gliomas after three-dimensional conformal radiotherapy. *J Clin Oncol* 2002;20:1635–1642.
5. Eric L. Chang, Serap Akyurek, Tedde Avalos, *et al.* Evaluation of peritumoral edema in the delineation of radiotherapy clinical target volumes for glioblastoma. *Int J Radiat Oncol Biol Phys* 2007;68:144–150.
6. Nelson DF, Curran WJ, Scott C, *et al.* Hyperfractionated radiation therapy and bis-chlorethyl nitrosourea in the treatment of malignant glioma—possible advantage observed at 72.0 Gy in 1.2 Gy B.I.D. fractions: Report of the Radiation Therapy Oncology Group Protocol 8302. *Int J Radiat Oncol Biol Phys* 1993;25:193–207.
7. Urtasun RC, Kinsella TJ, Farnan N, *et al.* Survival improvement in anaplastic astrocytoma, combining external radiation with halogenated pyrimidines: Final report of RTOG 86-12, Phase I-II study. *Int J Radiat Oncol Biol Phys* 1996;36:1163–1167.
8. Di Chiro G, DeLaPaz RL, Brooks RA, *et al.* Glucose utilization of cerebral gliomas measured by [^{18}F]fluorodeoxyglucose and positron emission tomography. *Neurology* 1982;32:1323–1329.
9. Patronas NJ, Brooks RA, DeLaPaz RL, *et al.* Glycolytic rate (PET) and contrast enhancement (CT) in human cerebral gliomas. *Am J Nucl Res* 1983;4:533–535.
10. Bergstrom M, Collins VP, Ehrin E, *et al.* Discrepancies in brain tumor extent as shown by computed tomography and positron emission tomography using [68Ga]EDTA [^{11}C]glucose, and [^{11}C]methionine. *J Comput Assist Tomogr* 1983;7:1062–1066.
11. Derlon JM, Bourdet C, Bustany P, *et al.* [^{11}C]l-methionine uptake in gliomas. *Neurosurgery* 1989;25:720–728.
12. Lilja A, Bergström K, Hartvig P, *et al.* Dynamic study of supratentorial gliomas with l-methyl-^{11}C-methionine and positron emission tomography. *Am J Neuroradiol* 1985;6:505–514.
13. Ogawa T, Shishido F, Kanno I, *et al.* Cerebral glioma: Evaluation with methionine PET. *Radiology* 1993;186:45–53.
14. Mosskin M, von Holst H, Bergström M, *et al.* Positron emission tomography with ^{11}C-methionine and computed tomography of intracranial tumours compared with histopathologic examination of multiple biopsies. *Acta Radiol* 1987;28:673–681.
15. Ericson K, Lilja A, Bergström M, *et al.* Positron emission tomography ([^{11}C]methyl)-l-methionine, [^{11}C]d-glucose, and [^{68}Ga]EDTA in supratentorial tumors. *J Comput Assist Tomograph* 1985;9:683–689.
16. Lilja A, Lundqvist H, Olsson Y, *et al.* Positron emission tomography and computed tomography in differential diagnosis between recurrent or residual glioma and treatment-induced brain lesions. *Acta Radiol* 1989;30:121–128.
17. Kaschten B, Stevenaert A, Sadzot B, *et al.* Preoperative evaluation of 54 gliomas by PET with fluorine-18-fluorodeoxyglucose and/or carbon-11-methionine. *J Nucl Med* 1998;39:778–785.
18. Mosskin M, Ericson K, Hindmarsh T, *et al.* Positron emission tomography compared with magnetic resonance imaging and computed tomography in supratentorial gliomas using multiple stereotactic biopsies as reference. *Acta Radiol* 1989;30:225–232.
19. Jansen EP, Dewit LG, van Herk M, Bartelink H. Target volumes in radiotherapy for high-grade malignant glioma of the brain. *Radiother Oncol* 2000;56:151–156.
20. Hatazawa J, Ishiwata K, Itoh M, *et al.* Quantitative evaluation of l-[methyl-C-11]methionine uptake in tumor using positron emission tomography. *J Nucl Med* 1989;30:1809–1813.
21. Curran WJ, Scott CB, Horton J, *et al.* Recursive partitioning analysis of prognostic factors in three Radiation Therapy Oncology Group malignant glioma trials. *J Natl Cancer Inst* 1993;85:704–710.
22. Hochberg HF, Pruitt A. Assumptions in the radiotherapy of glioblastoma. *Neurology* 1980;30:907–911.
23. Burger PC, Dubois PJ, Schold SC, *et al.* Computerized tomographic and pathologic studies of the untreated, quiescent, and recurrent glioblastoma multiforme. *J Neurosurg* 1983;58:159–169.

24. Halperin EC, Bentel G, Heinz ER, *et al.* Radiation therapy treatment planning in supratentorial glioblastoma multiforme: an analysis based on post mortem topographic anatomy with CT correlations. *Int J Radiat Oncol Biol Phys* 1989;17:1347–1350.
25. Kelly PJ, Daumas-Duport C, Kispert DB. Imaged-based stereotaxic serial biopsies in untreated intracranial glial neoplasm. *J Neurosurg* 1987;66:865–874.
26. Watanabe M, Tanaka R, Takeda N. Magnetic resonance imaging and histopathology of cerebral gliomas. *Neuroradiology* 1992;34:463–469.
27. Johnson PC, Hunt SJ, Drayer BP. Human cerebral gliomas: correlation of postmortem MR imaging and neuropathologic findings. *Radiology* 1989;170:211–217.
28. Giese A. Glioma invasion—pattern of dissemination by mechanisms of invasion and surgical intervention, pattern of gene expression and its regulatory control by tumor suppressor p53 and proto-oncogene ETS-1. *Acta Neurochir Suppl* 2003; 88:153–162.
29. Kelly PJ, Daumas-Duport C, Scheitauer BW. Stereotactic histologic correlations of CT- and MRI-defined abnormalities in patients with glial neoplasms. *Mayo Clin Proc* 1987;62:450–459.
30. Chamberlain MC, Murovic JA, Levin VA. Absence of contrast enhancement on CT brain scans of patients with supratentorial malignant gliomas. *Neurology* 1988;38:1371–1374.
31. Anca-Ligia Grosu, Wolfgang A. Weber, Eva Riedel, *et al.* l-(methyl-11C)Methionine positron emission tomography for target delineation in resected high-grade gliomas before radiotherapy. *Int J Radiat Oncol Biol Phys* 2005;63:64–74.
32. Ogawa T, Kanno I, Shishido F, *et al.* Clinical value of PET with ^{18}F-fluorodeoxyglucose and l-methyl-^{11}C-methionine for diagnosis of recurrent brain tumor and radiation injury. *Acta Radiol* 1991;21:198–202.

Cancer Science
The official journal of the Japanese Cancer Association JCA

Immunohistochemical analysis-based proteomic subclassification of newly diagnosed glioblastomas

Kazuya Motomura,[1] Atsushi Natsume,[1,11] Reiko Watanabe,[2] Ichiro Ito,[2] Yukinari Kato,[3] Hiroyuki Momota,[1] Ryo Nishikawa,[4] Kazuhiko Mishima,[4] Yoko Nakasu,[5] Tatsuya Abe,[6] Hiroki Namba,[7] Yoichi Nakazato,[8] Hiroshi Tashiro,[2] Ichiro Takeuchi,[9] Tsutomu Mori[10] and Toshihiko Wakabayashi[1]

[1]Department of Neurosurgery, Nagoya University School of Medicine, Nagoya; [2]Division of Diagnostic Pathology, Shizuoka Cancer Center, Shizuoka; [3]Molecular Tumor Marker Research Team, Faculty of Medicine, The Oncology Research Center, Advanced Molecular Epidemiology Research Institute, Yamagata University, Yamagata; [4]Department of Neurosurgery, Saitama Medical University International Center, Saitama; [5]Department of Neurosurgery, Shizuoka Cancer Center, Shizuoka; [6]Department of Neurosurgery, Oita University School of Medicine, Oita; [7]Department of Neurosurgery, Hamamatsu University School of Medicine, Hamamatsu; [8]Department of Human Pathology, Gunma University School of Medicine, Gunma; [9]Department of Engineering, Nagoya Institute of Technology, Nagoya; [10]Department of Human Lifesciences, Fukushima Medical University School of Nursing, Fukushima, Japan

(Received February 16, 2012/Revised June 20, 2012/Accepted June 21, 2012/Accepted manuscript online July 2, 2012/Article first published online August 6, 2012)

Recent gene expression and copy number profilings of glioblastoma multiforme (GBM) by The Cancer Genome Atlas (TCGA) Research Network suggest the existence of distinct subtypes of this tumor. However, these approaches might not be easily applicable in routine clinical practice. In the current study, we aimed to establish a proteomics-based subclassification of GBM by integrating their genomic and epigenomic profiles. We subclassified 79 newly diagnosed GBM based on expression patterns determined by comprehensive immunohistochemical observation in combination with their DNA copy number and DNA methylation patterns. The clinical relevance of our classification was independently validated in TCGA datasets. Consensus clustering identified the four distinct GBM subtypes: Oligodendrocyte Precursor (OPC) type, Differentiated Oligodendrocyte (DOC) type, Astrocytic Mesenchymal (AsMes) type and Mixed type. The OPC type was characterized by highly positive scores of Olig2, PDGFRA, p16, p53 and synaptophysin. In contrast, the AsMes type was strongly associated with strong expressions of nestin, CD44 and podoplanin, with a high glial fibrillary acidic protein score. The median overall survival of OPC-type patients was significantly longer than that of the AsMes-type patients (19.9 *vs* 12.8 months). This finding was in agreement with the Oncomine analysis of TCGA datasets, which revealed that PDGFRA and Olig2 were favorable prognostic factors and podoplanin and CD44 were associated with a poor clinical outcome. This is the first study to establish a subclassification of GBM on the basis of immunohistochemical analysis. Our study will shed light on personalized therapies that might be feasible in daily neuropathological practice. (*Cancer Sci* 2012; 103: 1871–1879)

Glioblastoma multiforme (GBM) is one of the most common and highly malignant brain tumors in the primary central nervous system in adults. GBM was one of the first tumor types registered in The Cancer Genome Atlas (TCGA), which is a project that catalogs genomic abnormalities involved in the development of cancer.[1,2] The techniques currently used in TCGA study for the detection of abnormalities include gene expression profiling, copy number variation profiling, single-nucleotide polymorphism genotyping, genome-wide methylation profiling,[3] microRNA profiling[4] and exon sequencing. Since the publication of the first TCGA Network paper,[1] several groups within the TCGA network have presented the results of highly detailed analyses of GBM. Verhaak *et al.*[5] recently subclassified GBM into Proneural, Neural, Classical and Mesenchymal subtypes by integrating multidimensional data on gene expression, somatic mutations and DNA copy number. The main features of the Proneural class are focal amplification of *PDGFRA*, *IDH1* mutation, and *TP53* mutation and/or loss of heterozygosity. Moreover, high expression of genes associated with oligodendrocyte development, such as *PDGFRA*, *NKX2-2* and *OLIG2*, were also associated with this subtype. The Neural subtype is characterized by the expression of neuron markers, such as *NEFL*, *GABRA1*, *SYT1* and *SLC12A5*. The Classical subtype features high *EGFR* expression associated with chromosome 7 amplification and low expression of *p16INK4A* and *p14ARF*, resulting from a focal 9p21.3 homozygous deletion. Neural stem cell markers, such as nestin, as well as components of the Notch and Sonic hedgehog signaling pathways, are highly expressed in the Classical type. The Mesenchymal subtype is characterized by focal hemizygous deletions at 17q11.2 that contains *NF1* and high expression of *YKL-40* (*CHI3L1*), *MET*, *CD44* and *MERTK*. This classification of GBM using gene expression profiles (TCGA) may address the important issue of the inability to define different patient outcomes on the basis of histopathological features. For ultimately establishing a simple classification of groups of patients with GBM according to clinicopathological factors, a protein-based immunohistochemical approach, which is routinely used in most neuropathology laboratories, needs to be applied to avoid more complex molecular biology techniques.[6]

In the present study, we analyzed 79 archival GBM samples by immunohistochemistry using antibodies against 16 proteins selected based on Verhaak's classification for immunohistochemical analysis-based GBM subclassification, including Proneural (Olig2, IDH1-R132H,[7] p53, PDGFRA and PDGFB), Neural (synaptophysin), Classical (p16, EGFR, Hes-1 and nestin) and Mesenchymal types (VEGF, YKL-40, CD44 and podoplanin [PDPN]), as well as high glial fibrillary acidic protein (GFAP) and Ki-67, and incorporated the results into the existing genomic and epigenomic data for these samples. We successfully identified clinically relevant subtypes that partially overlap the Verhaak subgroups.

Materials and Methods

Tumor samples. Samples from 79 consecutive patients with newly diagnosed GBM from several academic tertiary-care neurosurgical institutions were collected. All the samples were collected from GBM patients treated with temozolomide

[11]To whom correspondence should be addressed.
E-mail: anatsume@med.nagoya-u.ac.jp

doi: 10.1111/j.1349-7006.2012.02377.x

(TMZ). Paraffin-embedded surgical samples were collected for immunohistochemical analysis. All of the specimens had been fixed in 10% formalin. Three neuropathologists (Y.N., R.W. and I.I.) independently confirmed the GBM diagnosis according to WHO guidelines.[8,9]

Matched fresh-frozen tissue samples were also obtained. DNA was prepared as described previously.[10] All the patients provided their written informed consent for molecular studies of their tumor at each participating hospital. The study had the approval of each of the ethics committees of the Nagoya University Hospital, Shizuoka Cancer Center, Saitama Medical University Hospital, Oita University Hospital and Hamamatsu Medical University Hospital (title, "Genetic analysis associated with brain tumor"). This study complied with all the provisions of the Declaration of Helsinki.

Immunohistochemical analysis. Immunohistochemical analysis was performed as previously described.[11] The antibodies used in the present study are summarized in Table S1. For each immunostained slide, the percentage of positively stained GBM cells on a given slide was evaluated and scored, as shown in Table S2. This procedure was performed by two pathologists (R.W. and I.I.), and scores were decided through a consensus. This process was performed twice, and the final scores were determined at the second round before clustering analysis.

Multiplex ligation-dependent probe amplification. Multiplex ligation-dependent probe amplification (MLPA) was used for determining allelic losses and gains of the gene in the tumor samples. The analysis was performed using the SALSA MLPA kit P088-B1 and P105-C1 in accordance with the manufacturer's protocol (MRC Holland, Amsterdam, the Netherlands).[12–15] All the procedures were performed as described previously.[10]

Pyrosequencing. Tumor DNA was modified with bisulfate by using the EpiTect bisulfite kit (Qiagen, Courtaboeuf Cedex, France). Pyrosequencing technology was used to determine the methylation status of the CpG island region of MGMT, as described previously.[10,16,17]

***TP53* and *IDH1/IDH2* sequencing.** Direct sequencing of *TP53* exons 5–8, which contain mutation hot spots in gliomas, and *IDH1/2* was performed as previously described.[10,18–20] For IDH sequencing, 129 and 150-bp fragments spanning the sequences encoding the catalytic domains of *IDH1* (including codon 132) and *IDH2* (including codon 172), respectively, were amplified.

Oncomine data analysis. An independent set of 401 GBM mRNA expression profiles was analyzed by using the Oncomine Premium Research Edition to assess subtype reproducibility. Details of the standardized normalization techniques and statistical calculations can be found on the Oncomine website (https://www.oncomine.com).

Statistical analysis. To identify distinct GBM subclasses, we applied consensus clustering to our immunohistochemical data.[21] Consensus clustering has been used in many recent biomedical studies because it can estimate the statistical stability of the identified clusters.[5] Within the consensus clustering, *K*-means clustering with the Euclidean distance metric was used as the basic clustering option. For K ranging from 2 to 5, the *K*-means clustering was run over 10 000 iterations with a subsampling ratio of 0.8 for estimating the consensus matrix. For the purpose of visualization and cluster identification, hierarchical clustering with the Euclidean distance metric and the complete linkage option was applied to the estimated consensus matrix. The identified clusters were validated and confirmed using consensus cluster dependence factor plot analysis[21] and silhouette analysis.[22] To visualize the four identified clusters, principal component analysis (PCA) was applied to the immunohistochemical data and 3-D ellipsoids representing the covariance structure of each cluster were drawn in the 3-D plots of the first three principal components. Most of the statistical analyses (except the 3-D plot, which was generated by JMP ver.9.0) were performed using *R*.[23] We used a Kruskal–Wallis rank test to analyze the differences between the four GBM subgroups, and the pairwise differences in the expressions of 16 proteins and genetic/epigenetic alterations between each subgroup and the other three subgroups. The differences between the GBM subtypes with $P < 0.005$ were considered to be statistically significant in a more stringent manner, as the four clusters themselves are determined by the expression of these proteins and genetic/epigenetic alterations. Statistical analysis of survival was performed using the statistical software SPSS version 17.0 for Windows (SPSS, Chicago, IL, USA). Survival was estimated using the Kaplan–Meier method and survival curves were compared using the log-rank test.

Results

Patient characteristics. The summary of the GBM patient and treatment characteristics is shown in Table S3. All 79 patients received surgical treatment followed by standard TMZ-based chemotherapy and conventional radiation therapy, with daily concurrent TMZ at 75 mg/m^2 throughout the course of the radiation therapy.[24]

This study population included 50 male and 29 female patients aged 13–84 years (median age, 61 years). The median preoperative Eastern Cooperative Oncology Group performance status (ECOG PS) score at diagnosis was one (range, 0–4); the preoperative ECOG PS score was <1 in the case of 48 patients (60.8%). All the tumors were located in the supratentorial region: 60 tumors (75.9%) were located in the superficial area (cortical or subcortical area), and 19 (24.1%) were located in deep anatomical structures such as the basal ganglia and corpus callosum. Surgical gross total resection (GTR) was achieved in 24 patients (30.4%), and non-GTR was performed in 55 patients (69.6%).

Consensus clustering subclassifies four subtypes. The GBM subtypes identified by consensus clustering are shown in Figure 1, with clustering stability increasing from $K = 2$ to $K = 4$, but not to $K = 5$ (Figs 1,2). Furthermore, the identified clusters were confirmed on the basis of their positive silhouette width,[22] indicating higher similarity to their own class than to a member of any other class (Fig. 3).

According to the results, the 79 GBM cases examined were basically classified into four clusters: clusters I (nine cases), II (17 cases), III (14 cases) and IV (39 cases), depending on the branch length, which represents the correlation between the scoring data and the similarity in GBM tumor samples (Fig. 4). This analysis identified four discrete groups of sample sets that differed markedly in GBM protein expression. The 3-D ellipsoid of each cluster in PCA in Figure 5 also suggests the clear separations of each cluster. All the scores for the immunohistochemical analysis and genetic/epigenetic data lists for all the analyses are available in Table S4.

These protein groups were named according to the distribution and biological function of the representative protein expressions of Olig2, IDH1-R132H, PDGFRA, p16, EGFR, Hes-1, nestin, CD44, PDPN and GFAP; that is, Oligodendrocyte Precursor (OPC) type, Differentiated Oligodendrocyte (DOC) type, Astrocytic Mesenchymal (AsMes) type, and Mixed type. Figure 6 shows the immunohistochemical staining pattern in the 79 GBM cases, aligned according to the four identified clusters, indicating similarity in immunohistochemical staining patterns within each cluster.

Differentiated Oligodendrocyte type. All the samples clustered in this type showed high positivity for the oligodendroglial marker Olig2 and small round cell morphology (Table 1,

doi: 10.1111/j.1349-7006.2012.02377.x

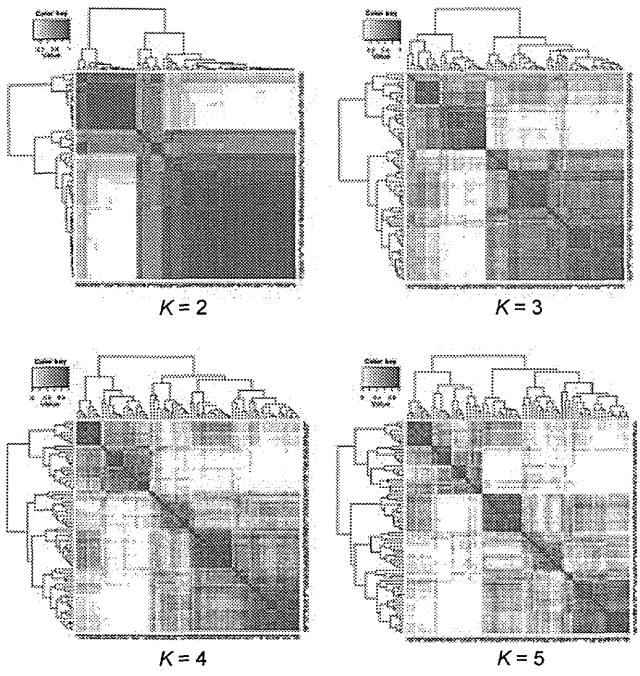

Fig. 1. Consensus matrix heat maps demonstrating the presence of several clusters within the 79 samples of GBM for $K = 2$ to $K = 5$ cluster assignments for each cluster method. The red areas identify the similarity between the samples and display samples clustered together across the bootstrap analysis.

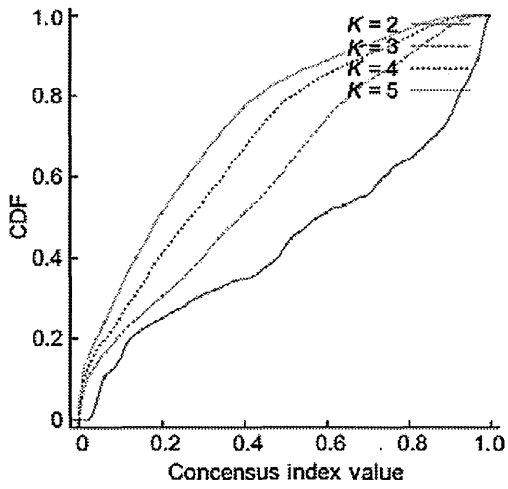

Fig. 2. Consensus clustering cluster dependence factor (CDF) for $K = 2$ to $K = 5$.

Fig. 6). Furthermore, negativity for p53 and p16 was noted. GFAP was almost always negative in the tumor cell cytoplasm (Fig. 6). Genetically, 1p/19q co-deletion and *CDKN2A* loss were more frequently observed in this cluster than in the other clusters (Fig. 7). The presence of 1p/19q co-deletion was assessed if the DNA copy numbers at a minimum of three adjacent loci were less than 0.65 at 1p and 19q.

Oligodendrocyte Precursor type. This cluster was characterized by highly positive scores for PDGFRA, p16, and p53 in addition to a highly positive score for an oligodendroglial marker, Olig2 (Fig. 6). From the perspective that oligodendrocytes arise during development from oligodendrocyte precursors,

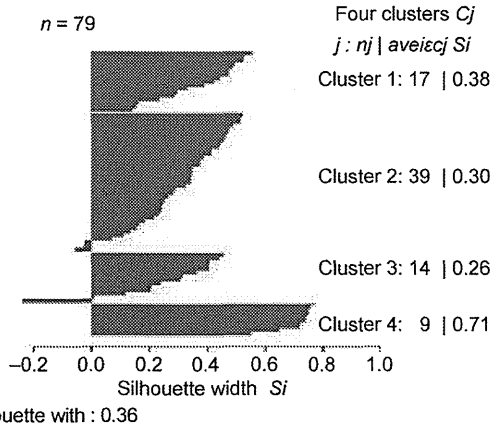

Fig. 3. Silhouette plot for identification of core samples.

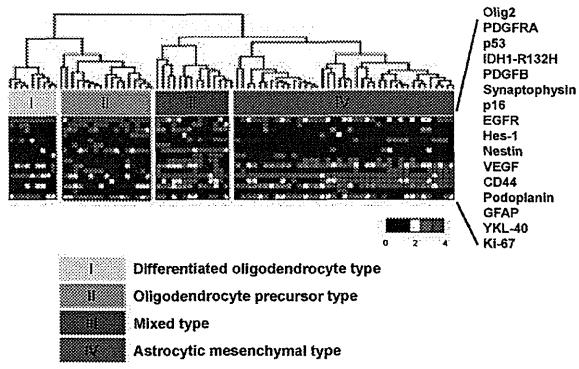

Fig. 4. Immunohistochemical analysis-based subgroups and comparison with genetic and epigenetic alterations. The heat map and dendrogram show the expression profiles of 16 proteins well characterized in glioblastoma multiforme (GBM) and demonstrate the significant pattern of differential expression among the four subgroups. The statistical significance of the differential protein expression was determined using one-way ANOVA.

which can be identified by the expression of a number of antigens, including PDGFRA, this subgroup was named the Oligodendrocyte Precursor (OPC) type. On the contrary, few samples had high scores for nestin, CD44, and PDPN in this group (Table 1; Fig. 6). It is interesting that the genetic alterations were observed in *IDH1* mutations (23.5%) and *TP53* mutations (52.9%). These findings were consistent with the results of protein expression. Methylation of the MGMT promoter (41.2%) was most frequently detected in this cluster (Fig. 7).

Astrocytic Mesenchymal type. This type was generally characterized by: strong membranous and/or stromal positivity for CD44 and/or PDPN; cytoplasmic positivity for GFAP and/or nestin in tumor cells; total negativity for p16, except in the case of four patients; and sparse positivity for p53 (Table 1, Fig. 6). Morphologically, the tumor cells observed in the H&E-stained sections showed pleomorphism. In striking contrast to the OPC type, this type was also strongly associated with low levels of Olig2, IDH1-R132H, p53, p16 and PDGFRA, and rather strong GFAP expression (Table 1). These findings suggest that this cluster was strongly characterized by astrocytic features.

Genetically, *IDH1* and *TP53* mutations were rare in this group. Furthermore, methylation of the MGMT promoter (20.5%) was detected at a low frequency (Fig. 7).

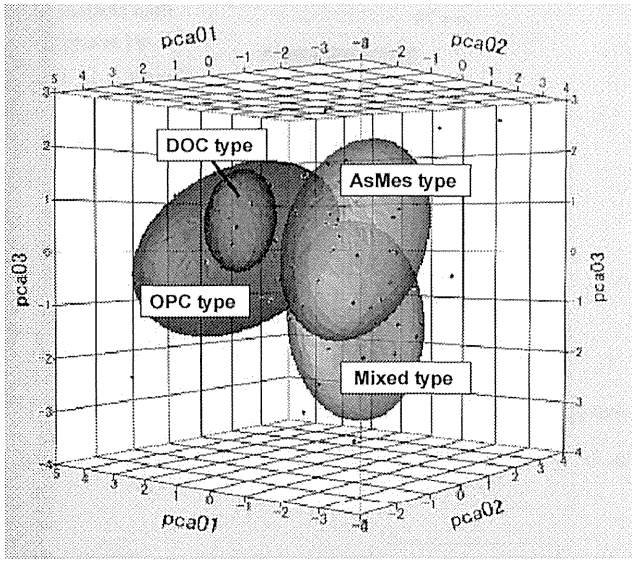

Fig. 5. Principal component analysis (PCA) of four glioblastoma multiforme (GBM) subtypes. Ellipsoid bodies represent two SD of the data distribution for each subgroup.

Mixed type. Compared with TCGA's Classical-type markers, frequent expressions of p16 (79%), EGFR (36%) and Hes-1 (64%), as well as a Proneural-type marker, p53 (64%), were predominant in this class (Table 1, Fig. 6).

Strong expression of the downstream Notch transcriptional target Hes-1 suggested that the prominent Notch-Hes-1 pathway was activated in this class. Furthermore, this cluster was characterized by positivity for CD44 and GFAP, and morphologically, by tumor cells with eosinophilic cytoplasm. This morphological characteristic was compatible with limited or scant positivity for Olig2. CD44 and PDPN were detected in many tumor cells.

In addition, this cluster had a genetically high frequency of *EGFR* amplification (57.1%) and low frequency of *CDKN2A* loss, and these findings are consistent with the protein expression data (Fig. 7). Thus, we named this cluster Mixed type because it shares characteristics of the OPC type and AsMes type or those of TCGA's Proneural and Classical types.

Morphological characteristics of the four types. On the H& E-stained sections, the morphological findings of the four types were fairly characteristic, although not specific (Fig. 8). In the DOC type, the tumor cells had small round or oval nuclei, scant cytoplasm and few cytoplasmic processes. The tumor cell nuclei showed a fine and diffuse chromatin (Fig. 8a,b). In some cases in which the tumor cells had faint processes, the cells tended to gather around vessels.

In the OPC type, in addition to small round or oval nucleated cells similar to those of the DOC type, there were scattered intermediate to large pleomorphic and/or multinucleated neoplastic cells, cells with vesicular chromatin, and/or cells with short spindle-shaped or irregularly-shaped nuclei that were slightly larger than the small round or oval cells (Fig. 8c,d).

In the AsMes type, many neoplastic cells had spindle-shaped nuclei and almost bipolar, distinct cytoplasmic processes. They were generally arranged in bundle-like and interlacing patterns. Some neoplastic cells had nuclei with vesicular open chromatin. The boundaries of the cytoplasmic processes were generally well defined (Fig. 8e,f).

In the Mixed type, there were scattered large pleomorphic cells on a background of intermediate or small cells. The latter background cells had irregularly-shaped nuclei and spindle-shaped cytoplasmic processes that were haphazardly arranged, in comparison with the bundle formations in the AsMes type (Fig. 8g,h).

Overview of the immunohistochemical data and genomic/epigenomic profiles across the four glioblastoma multiforme subtypes. We sought to select the most significant factors to distinguish the four GBM subgroups by a Kruskal–Wallis rank test. As indicated in Tables S5 and S6, the differences between the GBM subtypes showing $P < 0.005$ were considered to be statistically significant in a more stringent manner, as the four clusters themselves are determined by the expression of these proteins and genetic/epigenetic alterations. Of these, Olig2, p53, PDGFRA, synaptophysin, p16 and the *IDH1* mutation were positively correlated with the OPC type, whereas positive correlations with nestin, PDPN, CD44 and GFAP were predominant in the AsMes type. The DOC type showed a significant positive correlation with Olig2, and there was a significant positive correlation with the p16 expression in the Mixed type.

Proteomic clusters correlate with survival. The Kaplan–Meier survival analysis revealed that the four proteomic clusters differed significantly in their correlation with survival (Fig. 9 and Table 2). There were no significant differences in any of the clinical parameters (i.e. age, sex, preoperative ECOG PS, tumor location and extent of resection; Table S3) between the four cluster groups, as determined using the Fisher exact test.

It is interesting that the median overall survival (OS) associated with the OPC type was significantly longer (19.9 months [95% CI, 8.3–31.4]) than that of the patients with the AsMes type (12.8 months [95% CI, 10.0–15.7; $P = 0.041$]; Fig. 9). The difference was statistically significant, as determined by the log-rank test and univariate analysis. These findings were consistent with the OPC type being characterized by higher positive scores for IDH1-R132H (29%) in the immunohistochemical analysis and a high frequency of *IDH1* mutation (23.5%) in the genetic analysis, which are known to predict long-term survival.[25] Although the survival period of the patients in the Mixed type appeared to be the longest (median OS: 21.3 months [95% CI, 7.9–34.8]) among those of the other subgroups, the difference between these three subgroups was not statistically significant, presumably owing to the limited sample size in this study; the Kaplan–Meier curve of the DOC type (median OS: 14.8 months [95% CI, 2.6–27.0]) was similar to those of the OPC and Mixed types (Fig. 9).

Subgroup-specific outcome based on mRNA expression in The Cancer Genome Atlas datasets. An independent set of 401 GBM mRNA expression profiles was compiled from the Oncomine Premium Research Edition to assess subtype reproducibility. Among our selected 16 protein markers, information about the mRNA expressions of 12 markers and clinical outcomes could be obtained from TCGA brain dataset. IDH1-R132H, p53, p16 and Ki-67 were not available in the 401 GBM mRNA expression profiles of TCGA dataset because IDH1-R132H and p53 antibodies were used to detect mutation status, and this did not correlate with the mRNA expression of each gene. Moreover, because p16 protein expression correlates with the homozygous deletion of *CDKN2A*, we also excluded this protein from the analysis. In this analysis, the Olig2, PDGFB and PDGFRA mRNA expression levels were significantly low in the tumors of patients who died at 1 year compared with those who survived for 1 year after the treatment. Notably, PDGFRA was the most favorable prognostic factor among these factors ($P = 0.002$; Fig. 10 and Tables 3 and 4).

Furthermore, PDPN, CD44, YKL-40 and EGFR mRNA were significantly overexpressed in the tumors of the patients who died 1 year after the treatment. These results indicate that PDPN is significantly associated with a poor clinical outcome ($P = 0.0003$; Fig. 10).

doi: 10.1111/j.1349-7006.2012.02377.x

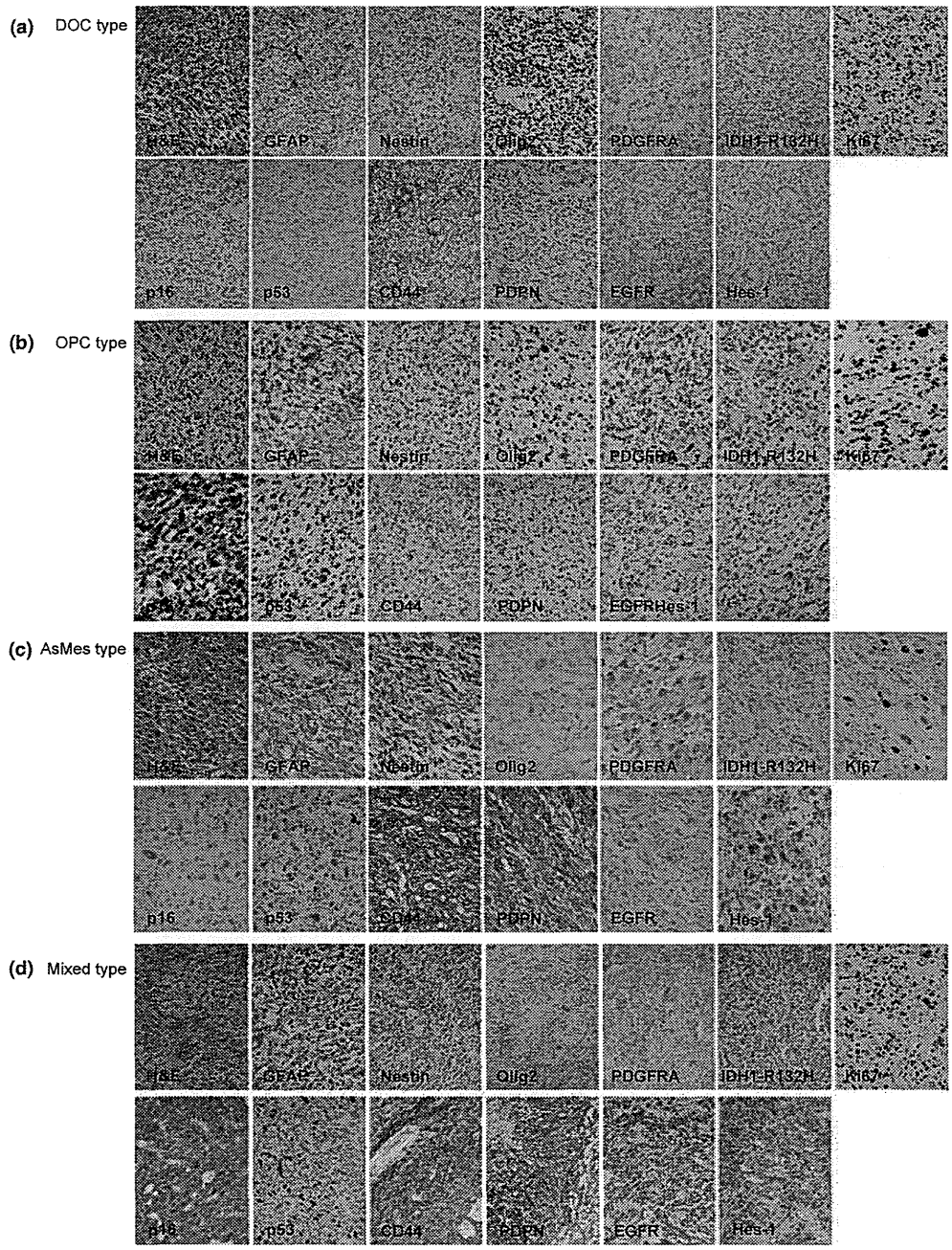

Fig. 6. Representative immunohistochemical images used in this study. (a) Differentiated Oligodendrocyte type (DOC type), glioblastoma multiforme (GBM) case.44. (b) Oligodendrocyte Precursor type (OPC type), GBM case.01. (c) Astorocytic Mesenchymal type (AsMes type), GBM case 03. (d) Mixed type, GBM case 04.

Discussion

A large number of studies have shown that GBM can be classified by gene and protein expression profiling.[5,26–28] The TCGA Research Network classifies GBM according to gene expression profiles into Proneural, Neural, Classical and Mesenchymal subtypes.[5] However, these transcriptomic approaches might not be easily applied in routine clinical practice because complicated techniques are necessary to perform several of the experiments. Compared with these approaches, an immunohistochemistry-based approach could have widespread utility in the clinical setting and lead to significantly improved patient stratification. The goal of the current study was to subclassify GBM using an immunohistochemical approach that is feasible in daily neuropathological practice, using a dataset from the TCGA Research Network as a reference. Our classification based on immunohistochemical analyses may enable the prediction of clinical chemosensitivity and survival in TMZ-treated patients with GBM.

Identification of four novel clusters by immunohistochemical analysis. We identified four novel clusters (OPC type, DOC type, AsMes type and Mixed type) with a considerably different expression profile of GBM tumors; to our knowledge, such an

Table 1. Frequency of positive score ≥3

Proteins	DOC type (n = 9) (%)	OPC type (n = 17) (%)	Mixed type (n = 14) (%)	AsMes type (n = 39) (%)	Total
Proneural					
Olig2	9 (100)	14 (82)	4 (29)	16 (41)	43
IDH1-R132H	0 (0)	5 (29)	0 (0)	1 (3)	6
p53	1 (11)	9 (53)	9 (64)	5 (13)	24
PDGFRA	3 (33)	10 (59)	5 (36)	3 (8)	21
PDGFB	2 (22)	1 (6)	5 (35)	9 (23)	17
Neural					
Synaptophysin	0 (0)	3 (18)	3 (21)	0 (0)	6
Classical					
p16	0 (0)	9 (53)	11 (79)	2 (5)	22
EGFR	0 (0)	0 (0)	5 (36)	5 (13)	10
Hes-1	0 (0)	3 (17	9 (64)	11 (28)	23
Nestin	2 (22)	2 (12)	4 (29)	24 (62)	32
Mesenchymal					
VEGF	1 (11)	6 (35)	4 (29)	11 (28)	22
YKL-40	0 (0)	1 (6)	0 (0)	2 (5)	3
Podoplanin	0 (0)	0 (0)	4 (29)	18 (46	22
CD44	5 (56)	1 (6)	11 (79)	37 (95)	54
GFAP	0 (0	3 (18)	10 (71)	32 (82)	45
Ki-67	5 (56)	11 (65)	5 (29)	18 (46)	39

AsMes, astrocytic mesenchymal; DOC, differentiated oligodendrocyte; OPC, oligodendrocyte precursor.

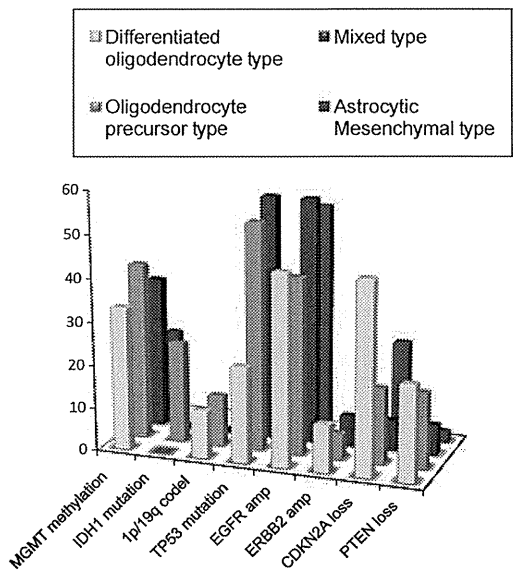

Fig. 7. Frequency and pattern of genetic and epigenetic alterations in four glioblastoma multiforme (GBM) subtypes.

expression profile has not been described elsewhere. However, the limitation of unsupervised clustering, which does not guarantee a clinically relevant classification, must be considered. Among the four clusters, the OPC and AsMes types in particular showed unique immunohistochemical patterns.

In addition, the survival patterns of the patients with GBM tumors classified into these types were significantly different. The OPC type was characterized by a favorable outcome and high positivity for Olig2, PDGFRA and IDH1-R132H on the immunohistochemical staining. The Kaplan–Meier log-rank test revealed that the OPC type was associated with a median

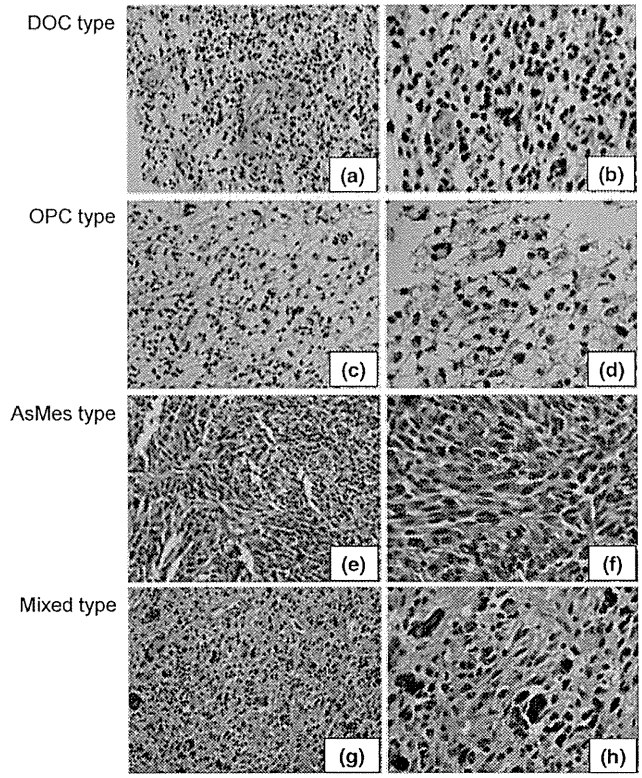

Fig. 8. Morphological findings of four types on the H&E sections. In the Differentiated Oligodendrocyte (DOC) type (original magnification: (a) ×20; (b) ×40), the tumor cells have small round/oval nuclei and indistinct processes. In the Oligodendrocyte Precursor (OPC) type (original magnification: (c) ×20; (d) ×40), there are scattered intermediate to large pleomorphic and/or multinucleated cells. In the Astrocytic Mesenchymal (AsMes) type (original magnification: (e) ×20; (f) ×40), spindle-shaped cytoplasmic processes are distinct and form bundles in an interlacing fashion. In the Mixed type (original magnification: (g) ×20; (h) ×40), in the background of small-sized to intermediate-sized spindle-shaped cells arranged in a haphazard fashion, there are several pleomorphic large cells.

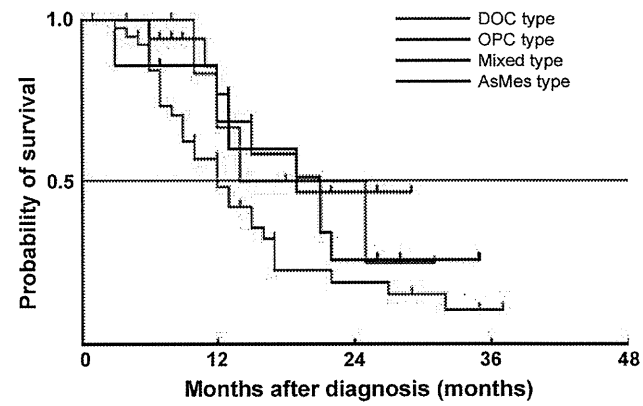

Fig. 9. Kaplan–Meier estimates of overall survival (OS) for all the glioblastoma multiforme (GBM) patients (n = 79) separated into four subgroups.

OS of 19.9 months (Fig. 9). This is possibly a result of the high positive score for IDH1-R132H, which is well recognized as a predictive biomarker and may influence this favorable sur-

doi: 10.1111/j.1349-7006.2012.02377.x

Table 2. Median overall survival of each of the four glioblastoma multiforme subtypes

	Median overall survival (months)	95% CI
Proteomic clusters		
OPC type	19.9†	8.3–31.4
DOC type	14.8	2.6–27.0
Mixed type	21.3	7.9–34.8
AsMes type	12.8	10.0–15.7

†The median overall survival of the OPC type was significantly longer (19.9 months [95% CI, 8.3–31.4]) than that of the AsMes type (12.8 months [95% CI, 10.0–15.7]) (P = 0.041). AsMes, astrocytic mesenchymal; DOC, differentiated oligodendrocyte. OPC, oligodendrocyte precursor.

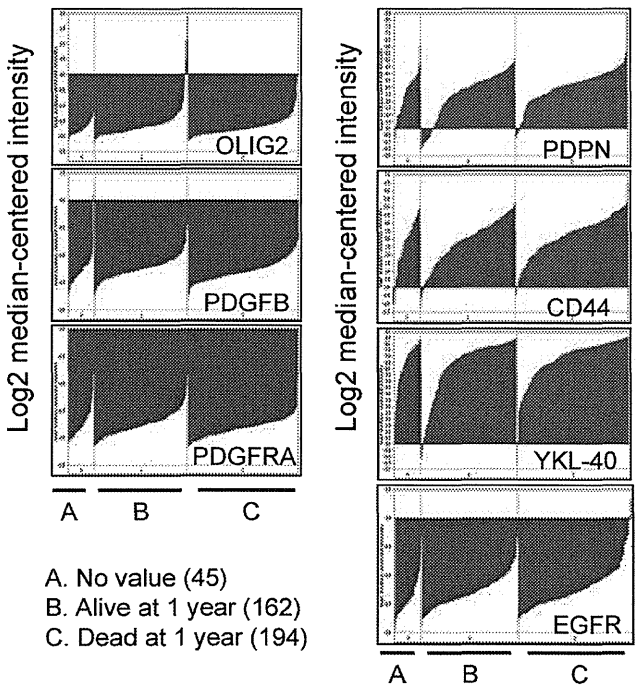

Fig. 10. Seven factors among our 16 markers that are correlated significantly with clinical outcomes from TCGA datasets. B and C show the log2 median-centered intensity of tumors of patients who were alive or dead at 1 year, respectively.

vival in GBM. Oligodendrocyte precursor cells are thought to develop from neural stem cells through multiple genetic and morphological changes.[29] Oligodendrocyte precursor cells express Olig1, Olig2, Sox10, Nkx2.2[30] and PDGFRA.[31,32] In particular, PDGFRA signaling is known to regulate the proliferation of oligodendrocyte precursor cells during neonatal development and regeneration in adulthood.[33]

In contrast, the characteristics of the AsMes type were high positivity for PDPN and CD44 in the stroma and GFAP in tumor cells. PDPN is a mucin-like transmembrane sialoglycoprotein putatively involved in migration, invasion, metastasis and malignant progression of several tumors, such as squamous cell carcinomas, mesothelioma and testicular tumors.[34–36] Furthermore, PDPN expression is thought to be associated with malignant progression of astrocytomas.[37] A study showed the presence of putative binding sites for NF1 within the basic transcription factor of the PDPN promoter lesion,[38] suggesting that NF1 negatively downregulates the expression of PDPN. CD44 is a major cell surface hyaluronan receptor and cancer stem cell marker that has been implicated in the progression of various cancer types.[39] Recently, CD44 was found to be upregulated in a broad range of GBM, and its elevated expression was correlated with poor prognosis.[40] An interesting finding is that CD44 and PDPN colocalize on cell surface protrusions in carcinoma cells, and the PDPN-CD44 interaction is important for driving directional cell migration in malignant tumors.[41]

The DOC type was clustered adjacent to the OPC type, suggesting that these clusters are closer to each other than to the other two clusters. A unique characteristic of the DOC type was that high positivity for Olig2 was observed in all the tumor sections in this cluster, whereas the positivity for the other markers was unremarkable. Genetically, the highest frequency of 1p/19q co-deletion, which refers to the combination of both 1p and 19q partial loss, and both hemizygous and homozygous deletions of the *CDKN2A* gene were observed in this class. This type is a heterogeneous group consisting of either 1p/19q co-deletion or *CDKN2A*-loss tumors. Taken together, this class may be differentiated into an oligodendroglioma-like lineage from oligodendrocyte precursor cells. The Mixed type was indeed mixed between the OPC and AsMes types. Moreover, PCA revealed that this type was a combination of the OPC and AsMes types.

Comparison with The Cancer Genome Atlas subclassification and validation of The Cancer Genome Atlas brain dataset. Mutations of the *IDH1* and *TP53* genes and high expression levels and high copy numbers of *PDFGRA* were frequently observed in the Proneural subtype advocated by Phillips and Verhaak,[5,26] suggesting that the OPC type is similar to the Proneural type. Striking characteristics common to the OPC type and the DOC type were high Olig2 expression and low

Table 3. Underexpression: dead at 1 year

Gene symbol	Reporter ID	*t*-test	*P*-value	*Q*-value	Fold change
OLIG2	213824_at	−2.105792	0.018113879	0.220443238	−1.0732534
PDGFB	217112_at	−2.3643584	0.009313148	0.188830637	−1.0354494
PDGFRA	211533_at	−2.8829412	0.002104464	0.141673037	−1.0440509

Table 4. Overexpression: dead at 1 year

Gene symbol	Reporter ID	*t*-test	*P*-value	*Q*-value	Fold change
PDPN	204879_at	3.4651806	3.04E-04	0.322990973	1.4722846
CD44	204490_s_at	2.6668687	0.004021729	0.527154075	1.296043
YKL-40	209395_at	2.2250252	0.013421925	0.672091602	1.3869164
EGFR	211551_at	1.8736842	0.030904011	0.840823061	1.0449007

expression levels of GFAP. However, the OPC type was characterized by higher positive scores for PDGFRA, p16, p53 and synaptophysin. The OPC type may be a mixture of Proneural and Neural subtypes.

In the Classical subtype, *EGFR* amplification and *CDKN2A* homozygous deletions were the frequent genetic alterations observed. Moreover, components of the nestin and Notch signaling pathways were highly expressed. According to our classification, overexpression of EGFR and the downstream effector of Notch signaling Hes-1 were most frequently observed in the Mixed type. Deletion of *CDKN2A* and downregulation of p16 were characteristic of the DOC type, and strong nestin expression was most frequently observed in the AsMes type. The Mesenchymal subtype was characterized by high expression levels of YKL-40 and MET and high frequency of *NF1* mutation/deletion. In our dataset, the mesenchymal markers PDPN and CD44 were highly expressed in the AsMes type, which is also characterized by strong GFAP expression. The combination of higher activity of mesenchymal and astrocytic markers is suggestive of an epithelial-to-mesenchymal transition.

In the present study, the outcomes of the patients with the OPC and AsMes types were significantly different. Contrary to Verhaak's classification, the outcomes of the patients with the OPC and AsMes types, on the basis of our classification, were significantly different.

Furthermore, we could easily distinguish these two subtypes using PDGFRA, p16, p53, PDPN and CD44, as well as the routinely used proteins, GFAP, Olig2, synaptophysin and nestin. The ability to discriminate these two subtypes will contribute to the development of different therapeutic approaches for each GBM subtype.

Although there were no independent validation samples of paraffin-embedded sections of GBM, determining the association between the expressions of these markers and the outcomes in 406 TCGA brain datasets would be of interest. Of note, Oncomine suggested that the overexpressions of PDPN and CD44 were associated with poor prognosis, and high expression levels of Olig2 and PDGFRA in tumor cells significantly improved the patient outcome. We are currently conducting a prospective randomized clinical trial, the Japan Clinical Oncology Group Study 0911, to validate the additive efficacy of interferon-β in 120 patients with newly diagnosed GBM.[42,43] It is anticipated that his clinical trial will validate our immunohistochemical approach.

In conclusion, the data obtained by expression profiling of 79 GBM tumors based on immunohistochemical studies suggest the existence of four proteomic subgroups of GBM tumors. To the best of our knowledge, this is the first study to establish the subclassification of GBM on the basis of immunohistochemical analysis. Among the four subtypes, the patients with the OPC type showed favorable outcomes. To develop more effective and less toxic GBM treatment regimens, it is necessary to identify and correctly classify the proteomic subtypes, as well as understand the underlying oncogenic driving pathways for each type.

Acknowledgments

The authors would like to thank Mr Akiyoshi Sakai (Clinical Laboratory, Kariya Toyota General Hospital, Kariya, Japan) and Mr Hideaki Maruse, Mr Takafumi Fukui and Mr. Yosuke Furui (FALCO Biosystems, Kyoto, Japan) for wonderful technical assistance.

Disclosure Statement

Kazuya Motomura was supported by a Grant-in-Aid (B) for Scientific Research from the Ministry of Health, Labor, and Welfare, Japan.

References

1 Network CGAR. Comprehensive genomic characterization defines human glioblastoma genes and core pathways. *Nature* 2008; **455**: 1061–8.
2 Parsons DW, Jones S, Zhang X *et al.* An integrated genomic analysis of human glioblastoma multiforme. *Science* 2008; **321**: 1807–12.
3 Noushmehr H, Weisenberger DJ, Diefes K *et al.* Identification of a CpG island methylator phenotype that defines a distinct subgroup of glioma. *Cancer Cell* 2010; **17**: 510–22.
4 Kim TM, Huang W, Park R, Park PJ, Johnson MD. A developmental taxonomy of glioblastoma defined and maintained by MicroRNAs. *Cancer Res* 2011; **71**: 3387–99.
5 Verhaak RG, Hoadley KA, Purdom E *et al.* Integrated genomic analysis identifies clinically relevant subtypes of glioblastoma characterized by abnormalities in PDGFRA, IDH1, EGFR, and NF1. *Cancer Cell* 2010; **17**: 98–110.
6 Northcott PA, Korshunov A, Witt H *et al.* Medulloblastoma comprises four distinct molecular variants. *J Clin Oncol* 2011; **29**: 1408–14.
7 Kato Y, Jin G, Kuan CT, McLendon RE, Yan H, Bigner DD. A monoclonal antibody IMab-1 specifically recognizes IDH1R132H, the most common glioma-derived mutation. *Biochem Biophys Res Commun* 2009; **390**: 547–51.
8 Louis DN, Ohgaki H, Wiestler OD *et al.* The 2007 WHO classification of tumours of the central nervous system. *Acta Neuropathol* 2007; **114**: 97–109.
9 Kleihues P, Cavenee WK. *WHO Classification of Tumours of the Central Nervous System*. Lyon: WHO Press, 2000.
10 Motomura K, Natsume A, Kishida Y *et al.* Benefits of interferon-beta and temozolomide combination therapy for newly diagnosed primary glioblastoma with the unmethylated MGMT promoter: a multicenter study. *Cancer* 2011; **117**: 1721–30.
11 Watanabe R, Nakasu Y, Tashiro H *et al.* O6-methylguanine DNA methyltransferase expression in tumor cells predicts outcome of radiotherapy plus concomitant and adjuvant temozolomide therapy in patients with primary glioblastoma. *Brain Tumor Pathol* 2011; **28**: 127–35.
12 Franco-Hernandez C, Martinez-Glez V, Alonso ME *et al.* Gene dosage and mutational analyses of EGFR in oligodendrogliomas. *Int J Oncol* 2007; **30**: 209–15.
13 Jeuken J, Cornelissen S, Boots-Sprenger S, Gijsen S, Wesseling P. Multiplex ligation-dependent probe amplification: a diagnostic tool for simultaneous identification of different genetic markers in glial tumors. *J Mol Diagn* 2006; **8**: 433–43.
14 Schouten JP, McElgunn CJ, Waaijer R, Zwijnenburg D, Diepvens F, Pals G. Relative quantification of 40 nucleic acid sequences by multiplex ligation-dependent probe amplification. *Nucleic Acids Res* 2002; **30**: e57.
15 Martinez-Glez V, Franco-Hernandez C, Lomas J *et al.* Multiplex ligation-dependent probe amplification (MLPA) screening in meningioma. *Cancer Genet Cytogenet* 2007; **173**: 170–2.
16 Natsume A, Wakabayashi T, Tsujimura K *et al.* The DNA demethylating agent 5-aza-2′-deoxycytidine activates NY-ESO-1 antigenicity in orthotopic human glioma. *Int J Cancer* 2008; **122**: 2542–53.
17 Oi S, Natsume A, Ito M *et al.* Synergistic induction of NY-ESO-1 antigen expression by a novel histone deacetylase inhibitor, valproic acid, with 5-aza-2′-deoxycytidine in glioma cells. *J Neurooncol* 2009; **92**: 15–22.
18 Nobusawa S, Watanabe T, Kleihues P, Ohgaki H. IDH1 mutations as molecular signature and predictive factor of secondary glioblastomas. *Clin Cancer Res* 2009; **15**: 6002–7.
19 Fults D, Brockmeyer D, Tullous MW, Pedone CA, Cawthon RM. p53 mutation loss of heterozygosity on chromosomes 17 and 10 during human astrocytoma progression. *Cancer Res* 1992; **52**: 674–9.
20 Hartmann C, Meyer J, Balss J *et al.* Type and frequency of IDH1 and IDH2 mutations are related to astrocytic and oligodendroglial differentiation and age: a study of 1,010 diffuse gliomas. *Acta Neuropathol* 2009; **118**: 469–74.
21 Monti S, Tamayo P, Mesirov J, Golub T. Consensus clustering: a resampling-based method for class discovery and visualization of gene expression microarray data. *Machine Learning* 2003; **52**: 91–118.
22 Rousseeuw PJ. Silhouettes – A graphical aid to the interpretation and validation of cluster-analysis. *J Comput Appl Math* 1987; **20**: 53–65.
23 Team RDC. *A Language and Environment for Statistical Computing*. Vienna, Austria: R Foundation for Statistical Computing, 2008.
24 Stupp R, Mason WP, van den Bent MJ *et al.* Radiotherapy plus concomitant and adjuvant temozolomide for glioblastoma. *N Engl J Med* 2005; **352**: 987–96.
25 Yan H, Parsons DW, Jin G *et al.* IDH1 and IDH2 mutations in gliomas. *N Engl J Med* 2009; **360**: 765–73.

doi: 10.1111/j.1349-7006.2012.02377.x

26 Phillips HS, Kharbanda S, Chen R *et al.* Molecular subclasses of high-grade glioma predict prognosis, delineate a pattern of disease progression, and resemble stages in neurogenesis. *Cancer Cell* 2006; **9**: 157–73.
27 Brennan C, Momota H, Hambardzumyan D *et al.* Glioblastoma subclasses can be defined by activity among signal transduction pathways and associated genomic alterations. *PLoS One* 2009; **4**: e7752.
28 Gravendeel LA, Kouwenhoven MC, Gevaert O *et al.* Intrinsic gene expression profiles of gliomas are a better predictor of survival than histology. *Cancer Res* 2009; **69**: 9065–72.
29 Nicolay DJ, Doucette JR, Nazarali AJ. Transcriptional control of oligodendrogenesis. *Glia* 2007; **55**: 1287–99.
30 Hu BY, Du ZW, Li XJ, Ayala M, Zhang SC. Human oligodendrocytes from embryonic stem cells: conserved SHH signaling networks and divergent FGF effects. *Development* 2009; **136**: 1443–52.
31 Levine JM, Reynolds R, Fawcett JW. The oligodendrocyte precursor cell in health and disease. *Trends Neurosci* 2001; **24**: 39–47.
32 Nishiyama A, Lin XH, Giese N, Heldin CH, Stallcup WB. Co-localization of NG2 proteoglycan and PDGF alpha-receptor on O2A progenitor cells in the developing rat brain. *J Neurosci Res* 1996; **43**: 299–314.
33 Rao RC, Boyd J, Padmanabhan R, Chenoweth JG, McKay RD. Efficient serum-free derivation of oligodendrocyte precursors from neural stem cell-enriched cultures. *Stem Cells* 2009; **27**: 116–25.
34 Kato Y, Kaneko M, Sata M, Fujita N, Tsuruo T, Osawa M. Enhanced expression of Aggrus (T1alpha/podoplanin), a platelet-aggregation-inducing factor in lung squamous cell carcinoma. *Tumour Biol* 2005; **26**: 195–200.
35 Kato Y, Sasagawa I, Kaneko M, Osawa M, Fujita N, Tsuruo T. Aggrus: a diagnostic marker that distinguishes seminoma from embryonal carcinoma in testicular germ cell tumors. *Oncogene* 2004; **23**: 8552–6.
36 Kato Y, Kaneko MK, Kuno A *et al.* Inhibition of tumor cell-induced platelet aggregation using a novel anti-podoplanin antibody reacting with its platelet-aggregation-stimulating domain. *Biochem Biophys Res Commun* 2006; **349**: 1301–7.
37 Mishima K, Kato Y, Kaneko MK, Nishikawa R, Hirose T, Matsutani M. Increased expression of podoplanin in malignant astrocytic tumors as a novel molecular marker of malignant progression. *Acta Neuropathol* 2006; **111**: 483–8.
38 Hantusch B, Kalt R, Krieger S, Puri C, Kerjaschki D. Sp1/Sp3 and DNA-methylation contribute to basal transcriptional activation of human podoplanin in MG63 versus Saos-2 osteoblastic cells. *BMC Mol Biol* 2007; **8**: 20.
39 Stamenkovic I, Yu Q. Shedding light on proteolytic cleavage of CD44: the responsible sheddase and functional significance of shedding. *J Invest Dermatol* 2009; **129**: 1321–4.
40 Xu Y, Stamenkovic I, Yu Q. CD44 attenuates activation of the hippo signaling pathway and is a prime therapeutic target for glioblastoma. *Cancer Res* 2010; **70**: 2455–64.
41 Martin-Villar E, Fernandez-Munoz B, Parsons M *et al.* Podoplanin associates with CD44 to promote directional cell migration. *Mol Biol Cell* 2010; **21**: 4387–99.
42 Wakabayashi T, Kayama T, Nishikawa R *et al.* A multicenter phase I trial of interferon-beta and temozolomide combination therapy for high-grade gliomas (INTEGRA Study). *Jpn J Clin Oncol* 2008; **38**: 715–8.
43 Wakabayashi T, Kayama T, Nishikawa R *et al.* A multicenter phase I trial of combination therapy with interferon-beta and temozolomide for high-grade gliomas (INTEGRA study): the final report. *J Neurooncol* 2011; **104**: 573–7.

Supporting Information

Additional Supporting Information may be found in the online version of this article:

Table S1. Antibodies and immunostaining conditions.

Table S2. Scoring system for immunohistochemical positivity used in this study.

Table S3. Clinical characteristics of the four GBM subtypes.

Table S4. Scores of all immunohistochemical analysis and genetic/epigenetic data lists for all the analyses.

Table S5. Significant pairwise correlation coefficients derived from the Kruskal–Wallis rank test of the expressions of 16 proteins in the four GBM subgroups.

Table S6. Significant pairwise correlation coefficients derived from the Kruskal–Wallis rank test of the genetic and epigenetic alterations in the four GBM subgroups.

Please note: Wiley-Blackwell are not responsible for the content or functionality of any supporting materials supplied by the authors. Any queries (other than missing material) should be directed to the corresponding author for the article.

Cancer Science
The official journal of the Japanese Cancer Association

Significance of *IDH* mutations varies with tumor histology, grade, and genetics in Japanese glioma patients

Akitake Mukasa,[1,9] Shunsaku Takayanagi,[1] Kuniaki Saito,[1] Junji Shibahara,[2] Yusuke Tabei,[3] Kazuhide Furuya,[4] Takafumi Ide,[5] Yoshitaka Narita,[6] Ryo Nishikawa,[7] Keisuke Ueki[8] and Nobuhito Saito[1]

Departments of [1]Neurosurgery, [2]Pathology, University of Tokyo, Tokyo; [3]Department of Neurosurgery, Tokyo Metropolitan Cancer and Infectious Diseases Center Komagome Hospital, Tokyo; [4]Department of Neurosurgery, Teikyo University School of Medicine, Tokyo; [5]Department of Neurosurgery, Tokyo Metropolitan Bokutoh Hospital, Tokyo; [6]Department of Neurosurgery and Neuro-Oncology, National Cancer Center Hospital, Tokyo; [7]Department of Neuro-Oncology/Neurosurgery, International Medical Center, Saitama Medical University, Saitama; [8]Department of Neurosurgery, Dokkyo University School of Medicine, Tochigi, Japan

(Received October 20, 2011/Revised November 24, 2011/Accepted November 29, 2011/Accepted manuscript online December 2, 2011/Article first published online January 13, 2012)

Mutations in isocitrate dehydrogenase 1 (*IDH1*) and *IDH2* are found frequently in malignant gliomas and are likely involved in early gliomagenesis. To understand the prevalence of these mutations and their relationship to other genetic alterations and impact on prognosis for Japanese glioma patients, we analyzed 250 glioma cases. Mutations of *IDH1* and *IDH2* were found in 73 (29%) and 2 (1%) cases, respectively. All detected mutations were heterozygous, and most mutations were an Arg132His (G395A) substitution. *IDH* mutations were frequent in oligodendroglial tumors (37/52, 71%) and diffuse astrocytomas (17/29, 59%), and were less frequent in anaplastic astrocytomas (8/29, 28%) and glioblastomas (13/125, 10%). The pilocytic astrocytomas and gangliogliomas did not have either mutation. Notably, 28 of 30 oligodendroglial tumors harboring the 1p/19q co-deletion also had an *IDH* mutation, and these alterations were significantly correlated ($P < 0.001$). The association between *TP53* and *IDH* mutation was significant in diffuse astrocytomas ($P = 0.0018$). *MGMT* promoter methylation was significantly associated with *IDH* mutation in grade 2 ($P < 0.001$) and grade 3 ($P = 0.02$) gliomas. *IDH* mutation and 1p/19q co-deletion were independent favorable prognostic factors for patients with grade 3 gliomas. For patients with grade 3 gliomas and without 1p/19q co-deletion, *IDH* mutation was strongly associated with increased progression-free survival ($P < 0.0001$) and overall survival ($P < 0.0001$), but no such marked correlation was observed with grade 2 gliomas or glioblastomas. Therefore, *IDH* mutation would be most useful when assessing prognosis of patients with grade 3 glioma with intact 1p/19q; anaplastic astrocytomas account for most of these grade 3 gliomas. (*Cancer Sci* 2012; 103: 587–592)

Gliomas are among the most common and formidable brain tumors.[1] Despite intensive treatment, most patients die within 2-10 years. Therefore, development of novel therapeutic strategies based on greater understanding of tumor characteristics is needed. Recently, a comprehensive sequence analysis of human GBM that included most human genes revealed frequent mutations in *IDH1*.[2] Subsequent analyses revealed that these mutations occur more frequently in low-grade glioma than in GBM, with a rate of *IDH1* mutation as high as 59–90%.[3–7] The *IDH* gene mutation is currently believed to occur in the early stage of gliomagenesis[4,6] and to play a critical role in tumor development.

The *IDH* genes encode redox enzymes; these enzymes convert isocitrate to alpha-ketoglutarate, use NAD(P)+ as a coenzyme, and function in energy metabolism. There are three *IDH* genes in humans, and only mutations in *IDH1* are frequently found in gliomas; the IDH1 enzyme resides in the cytosol and peroxisomes.[2–7] Mutations in *IDH2* are rare in gliomas; IDH2 localizes to mitochondria and functions in the Krebs (citric acid) cycle. To date, no *IDH3* mutation has been reported. Most *IDH1* mutations in gliomas are missense mutations at amino acid 132, which is in the catalytic domain and binds to substrate. Similarly, *IDH2* mutations in gliomas are substitutions at amino acid 172, which is functionally equivalent to amino acid 132 of IDH1. *IDH1* and *IDH2* mutations in the catalytic domain are also found in 8–23% of acute myeloid leukemias.[8,9] Mutations in *IDH* genes are rarely found in other tumors.[7,10]

In general, a tumor with an *IDH* mutation has either an *IDH1* or *IDH2* mutation, and the mutation is heterozygous with a wild-type allele.[2,4,6,7] This observation led to the notion that mutated *IDH1/IDH2* genes gain novel functions and are oncogenes, and that the wild-type *IDH* genes are not tumor suppressor genes. In fact, mutant IDH1 has novel enzymatic activity; it converts alpha-ketoglutarate to 2-HG, and accumulated 2-HG is presumed to contribute to tumorigenesis as an "oncometabolite".[9,11–13]

Malignant gliomas categorized as WHO grade 4[2,5,7,14,15] or grade 3[5,7,15–17] with an *IDH* mutation were reportedly associated with higher PFS[15–17] and OS[2,5,7,14–17] than those without an *IDH* mutation. However, for grade 2 gliomas, the relation between the presence of an *IDH* mutation and prognosis is controversial.[15,18–20]

The *IDH* mutations apparently have an important role in many aspects of glioma, including gliomagenesis, patient prognosis, and development of therapeutic strategies. However, information on *IDH* mutations in gliomas, such as prevalence, relation to other genetic alterations, and prognostic value, is still limited, particularly for Asian populations,[21,22] including Japanese patients.[5,17] Thus, to further clarify the significance of *IDH* mutations with regard to proper diagnosis and optimized treatment of malignant gliomas, we sought basic data on a large number of Japanese glioma patients for *IDH1* and *IDH2* mutations and other genetic and epigenetic alterations frequently found in gliomas, specifically 1p/19q LOH, *TP53* mutation, and *MGMT* promoter methylation.

Materials and Methods

Tumor specimens. Tumor samples and paired blood samples were obtained following surgery. Of 250 gliomas, 168 tumors were collected at the University of Tokyo hospital (Tokyo,

[9]To whom correspondence should be addressed.
E-mail: mukasa-nsu@umin.ac.jp

doi: 10.1111/j.1349-7006.2011.02175.x

Japan) and 82 gliomas were collected at collaborating hospitals. The study was approved by the Ethics Committee of the University of Tokyo and all patients gave written informed consent. Histological diagnoses were made on formalin-fixed, paraffin-embedded tissues following the WHO classification[1] by a neuropathologist (J.S.) for samples from the University of Tokyo hospital and consensus diagnoses were made by four neuropathologists for samples from other hospitals as reported previously.[23] Genomic DNA was extracted for genetic analyses. Patients with the same grade (2, 3, or 4) glioma were treated similarly with surgical resection followed by radiotherapy and alkylating agent chemotherapy.

Genetic analysis. For *IDH* gene mutations, the genomic regions spanning the catalytic domain of *IDH1*, including codon 132, and of *IDH2*, including codon 172, were analyzed by direct sequencing using the Genetic Analyzer 310 (Applied Biosystems, Foster City, CA, USA). An aliquot of DNA was amplified by PCR using AmpliTaq Gold (Applied Biosystems) with annealing temperature at 55°C. The primers 5′-TGCCACCAACGACCAAGTCA and 5′-TGTGTTGAGATGGACGCCTATTTG were used for *IDH1* amplification and sequencing, as reported previously.[15] Amplification of *IDH2* was carried out using the primers 5′-CTCTGTCCTCACAGAGTTCAAGC and 5′-CCACTCCTTGACACCACTGCC, and the *IDH2* sequencing reactions were carried out using the primers 5′-AAGTCCCAATGGAACTATCCG and 5′-TCTGTGGCCTTGTACTGCAGAG.

Loss of heterozygosity on chromosomes 1p and 19q was determined using microsatellite analysis as described previously.[23] When tumors had no available paired blood DNA or when the LOH assay was ambiguous because of non-informative microsatellite markers, MLPA assay was carried out using the SALSA MLPA kit P088 (MRC Holland, Amsterdam, the Netherlands) following the manufacturer's instructions. *TP53* gene mutation was determined by direct sequencing following PCR-SSCP screening of exons 5–8 of *TP53*, as described previously.[24]

Methylation-specific PCR. Genomic DNA samples (250 ng each) were used for bisulfite reactions using the EZ DNA Methylation Kit (Zymo Research, Irvine, CA, USA) according to the manufacturer's protocol. DNA methylation status of the *MGMT* promoter was then determined by methylation-specific PCR as described by Esteller *et al.*[25]

Statistical analysis. Fisher's exact test was used to compare the genotype distributions. Overall survival was defined as the time between initial surgery and death or last follow-up. Progression-free survival was defined as the time between initial surgery and recurrence or last follow-up. Both OS and PFS were calculated according to the Kaplan–Meier method, and differences among patient subsets were evaluated using the log–rank test. Statistical calculations were carried out using JMP 9 (SAS Institute, Cary, NC, USA).

Results

Frequency and characteristics of *IDH* mutations in glioma samples from Japanese patients. We analyzed 250 human glioma samples obtained following surgery; these tumors consisted of 125 GBM, 29 AA, 29 DA, 52 oligodendroglial tumors, 9 PA, and 6 GGL. Mutations of *IDH1* and *IDH2* were found in 73 (29%) and 2 (1%) tumors, respectively. All detected mutations were heterozygous, missense mutations. Among the 73 *IDH1* mutations, the G395A (R132H) substitution was the most frequent mutation (occurring in 70/73 cases, 96%), C394A (R132S) substitutions occurred in two cases, and a C394T (R132C) substitution occurred in one case. Of the two *IDH2* mutations, one was a G515A (R172K) substitution, and the other was an A514T (R172W) substitution. *IDH* mutations (*IDH1* or *IDH2*) were found in 13 (10%) of 125 GBM, 8 (28%) AA, 17 (59%) DA, and in 37 (71%) oligodendroglial tumors (Table 1). In the 52 oligodendroglial tumors, *IDH* mutations were found in 19/25 (76%) OG, 4/7 (57%) OA, 10/15 (67%) AOG, and 4/5 (80%) AOA. No mutation was detected in any case of PA or GGL. A higher rate of *IDH* mutation was found in secondary GBM (6/13, 46%) than primary GBM (6/109, 6%). In the three GBMO cases, there was only one *IDH1* mutation.

Association between *IDH* mutation and 1p/19q co-deletion, *TP53* mutation, or *MGMT* promoter methylation. The frequencies of 1p/19q co-deletion and *TP53* mutation and their relationship with *IDH* mutations are shown in Table 1. As expected, 1p/19q co-deletion was common in oligodendroglial tumors, especially those without an astrocytic component (OG 76%, AOG 67%), whereas *TP53* mutations were common in lower-grade astrocytomas (DA 45%); these genetic aberrations were never coincident. In OG, 1p/19q co-deletion was significantly correlated with *IDH* mutation ($P < 0.001$), and almost all oligodendroglial tumors with 1p/19q co-deletion had an *IDH* mutation (28/30, 93%).

The *TP53* mutation was more prevalent in DA (45%) than in AA (34%) or primary GBM (22%). However, when *IDH* mutation was present, *TP53* mutation was more frequent, and *TP53* mutations were found in 12/17 (71%) DA, 5/8 (63%) AA, and 3/6 (50%) primary GBMs that also had an *IDH* mutation. The rates of *IDH* mutation in astrocytic tumors with *TP53* mutation were higher than those with wild-type *TP53* (92% *vs* 31% in DA, 50% *vs* 16% in AA, and 13% *vs* 4% in primary GBM), and the association between *TP53* and *IDH* mutation was significant in DA ($P = 0.0018$), but not in AA or GBM. The majority of DA tumors with *TP53* mutation had *IDH* mutation (12/13, 92%); in contrast, only a few primary GBM tumors with *TP53* mutation also had an *IDH* mutation (3/23, 13%).

Of a total 250 gliomas, *MGMT* promoter methylation status was analyzed for 132 gliomas (grade 2, 3, and 4) resected at the University of Tokyo hospital. Methylation was evident in 37/69 GBM (54%), 5/18 AA (28%), 10/17 DA (59%), 8/10 AOG/AOA (80%), and 13/18 OG/OA (72%) (Table 1). The association between *IDH* mutation and *MGMT* methylation was significant in grade 2 ($P < 0.001$) and grade 3 gliomas ($P = 0.02$), but not in grade 4 gliomas ($P = 0.11$).

Prognostic value of *IDH* mutation and other genetic alterations. We evaluated the potential prognostic value of *IDH* mutation and other genetic alterations in WHO grade 2, 3, and 4 gliomas. For patients with grade 2 gliomas, univariate analysis showed that *IDH* mutation was not associated with OS ($P = 0.07$) or PFS ($P = 0.29$). Codeleted 1p/19q and wild-type *TP53* each slightly correlated with increased PFS ($P = 0.014$ and $P = 0.029$, respectively), but they were not correlated with OS, and neither of these genetic alterations showed significant association with prognosis in multivariate analysis (Table 2). *MGMT* promoter methylation was also not associated with prognosis. Similarly, we did not observe a significant association of *IDH* mutation with better prognosis for DA (OS, $P = 0.10$; PFS, $P = 0.58$).

In grade 3 gliomas, univariate analysis showed that the association between *IDH* mutation and prolonged survival (OS, $P = 0.0004$; PFS, $P < 0.0001$) was significant and that 1p/19q co-deletion was associated with prolonged survival (OS, $P = 0.028$; PFS, $P = 0.0025$), but that neither *TP53* mutation nor *MGMT* promoter status was associated with prognosis. Although *IDH* mutation and 1p/19q co-deletion were tightly associated with one another, the multivariate analysis further indicated that these alterations were independent indicators of a favorable prognosis (Table 2). *IDH* mutation was present in almost all tumors with the 1p/19q co-deletion.[26] Therefore, grade 3 gliomas were divided into three genetic subgroups: (i) 1p/19q codeleted tumors, most of which carry *IDH* mutation and show oligodendroglial phenotype; (ii) tumors without 1p/19q co-deletion and with mutant *IDH*; and (iii) tumors

doi: 10.1111/j.1349-7006.2011.02175.x

Table 1. *IDH* mutation and common genetic and epigenetic alterations in gliomas from Japanese patients

Tumor pathology (WHO grade) *IDH1* or *IDH2* status	No. of patients	Frequency of *IDH1* or *IDH2* mutation	Median age, years	Male sex (%)	1p/19q co-deletion	*TP53* mutation	Methylated *MGMT* promoter (%)
GBM primary (Gr. 4)	109	6/109 (6%)	62	61	1	23 (22%)	27/57 (47)
Mutant	6		43	50	1	3 n.s.	1/1 (100)
Wild-type	103		62	61	0	20	26/56 (46)
GBM secondary (Gr. 4)	13	6/13 (46%)	47	69	0	2 (15%)	7/9 (78)
Mutant	6		52	50	0	2 n.s.	4/5 (80)
Wild-type	7		43	86	0	0	3/4 (75)
GBMO (Gr.4)	3	1/3 (33%)	80	67	1	0	3/3 (100)
Mutant	1		62	100	1	0	1/1 (100)
Wild-type	2		80	50	0	0	2/2 (100)
Anaplastic astrocytoma (Gr. 3)	29	8/29 (28%)	57	55	1	10 (34%)	5/18 (28)
Mutant	8		46	50	1	5 n.s.	2/5 (40)
Wild-type	22		60	57	0	5	3/13 (23)
Anaplastic oligoastrocytoma (Gr. 3)	5	4/5 (80%)	43	40	0	4 (80%)	2/3 (66)
Mutant	4		48	25	0	3 n.s.	2/2 (100)
Wild-type	1		11	100	0	1	0/1 (0)
Anaplastic oligodendroglioma (Gr. 3)	15	10/15 (67%)	62	56	10 (67%)	0	6/7 (86)
Mutant	10		49	43	9*	0	5/5 (100)
Wild-type	5		66	100	1	0	1/2 (50)
Diffuse astrocytoma (Gr. 2)	29	17/29 (59%)	32	61	3	13 (45%)	10/17 (59)
Mutant	17		33	59	2	12***	10/10 (100)
Wild-type	12		30	64	1	1	0/7 (0)
Oligoastrocytoma (Gr. 2)	7	4/7 (57%)	44	71	1	1	5/6 (83)
Mutant	4		37	100	1	1	3/3 (100)
Wild-type	3		53	33	0	0	2/3 (67)
Oligodendroglioma (Gr. 2)	25	19/25 (76%)	46	52	19 (76%)	3	8/12 (66)
Mutant	19		47	53	18**	1	7/10 (70)
Wild-type	6		34	50	1	2	1/2 (50)
Pilocytic astrocytoma (Gr. 1)	9	0%	12	56	0	0	N/A
Mutant	0		N/A	N/A	0	0	
Wild-type	9		12	56	0	0	
Ganglioglioma (Gr. 1)	6	0%	22	67	0	0	N/A
Mutant	0		N/A	N/A	0	0	
Wild-type	6		22	67	0	0	

*P = 0.0037; **P = 0.0001; ***P = 0.0018. The association with *IDH* mutation (Fisher's exact test). GBM, glioblastoma; GBMO, glioblastoma with oligodendroglioma component; N/A, not analyzed; n.s., not significant.

Table 2. Prognostic value of common genetic alterations for overall survival (OS) and progression-free survival (PFS) in gliomas (multivariate analysis)

	PFS			OS		
	P-value	Hazard ratio	95% CI	*P*-value	Hazard ratio	95% CI
Grade 2 glioma						
IDH mutation	0.4408	0.602	0.1678–2.1535	0.1573	0.329	0.0728–1.5270
1p/19q co-deletion	0.3591	0.495	0.1083–2.2020	0.7988	1.237	0.2353–6.0194
TP53 mutation	0.2904	2.036	0.5526–7.7157	0.4693	0.537	0.0685–2.6350
Grade 3 glioma						
IDH mutation	<0.0001†	0.059	0.0086–0.2395	0.0403†	0.319	0.0985–0.9519
1p/19q co-deletion	0.0016†	0.055	0.0025–0.3904	0.0170†	0.184	0.0271–0.7567
TP53 mutation	0.4144	0.646	0.2045–1.7994	0.0300†	0.294	0.0786–0.8937
Primary GBM						
IDH mutation	0.8456	0.898	0.2575–2.4255	0.8560	0.905	0.2609–2.4203
TP53 mutation	0.1533	0.605	0.2792–1.1944	0.3089	0.705	0.3354–1.3613
Methylated *MGMT* promoter	0.0031†	0.407	0.2216–0.7375	0.0058†	0.429	0.2324–0.7820

†Significant value. Cox proportional hazard modeling for OS or PFS was applied for the major variable for prognostic factors. CI, confidence interval; GBM, glioblastoma.

without 1p/19q co-deletion and with wild-type *IDH*. Grade 3 gliomas were assessed with regard to the association between the genetic alterations and disease course (Fig. 1). In these genetic subgroups, grade 3 gliomas without 1p/19q co-deletion and with wild-type *IDH* were revealed to have markedly worse OS ($P < 0.0001$) (Fig. 1C) and PFS ($P < 0.0001$) (Fig. 1D), but

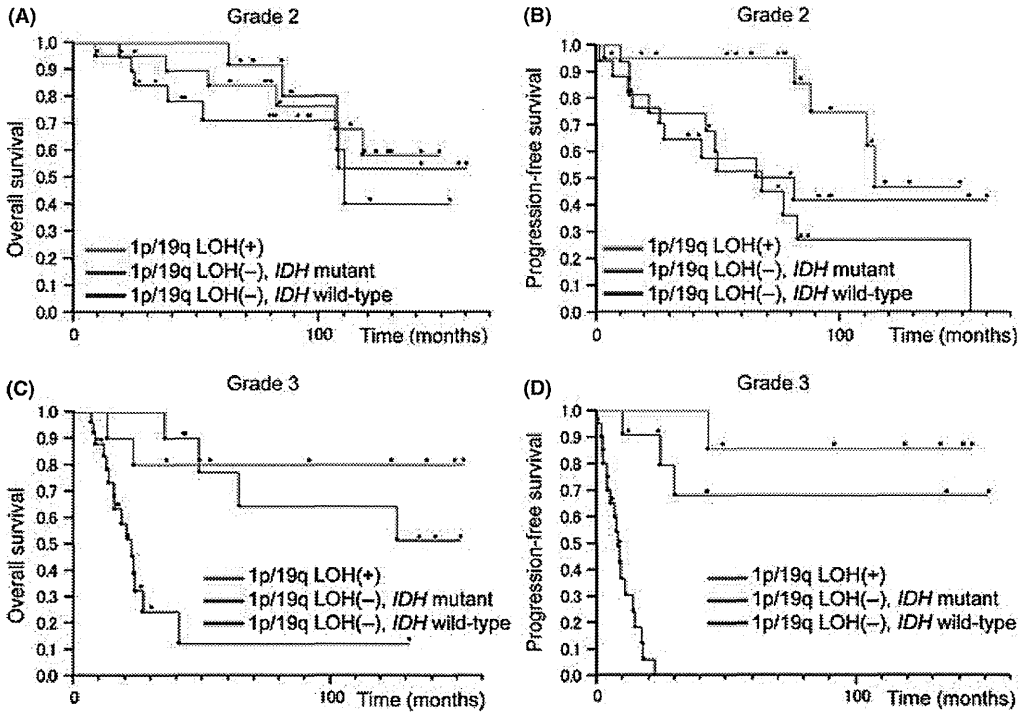

Fig. 1. Overall survival (OS) and progression-free survival (PFS) curves for patients with grade 2 and 3 gliomas with or without 1p/19q loss of heterozygosity (LOH) and/or isocitrate dehydrogenase (*IDH*) mutation. Overall survival (A) and PFS (B) in grade 2 gliomas; OS (C) and PFS (D) in grade 3 gliomas.

these lower survival rates were not observed for patients with grade 2 gliomas lacking 1p/19q co-deletion and *IDH* mutation (Fig. 1A,B). Grade 3 gliomas without 1p/19q co-deletion were predominantly AA (28 AAs, 5 AOAs, and 5 AOGs), and only 1 AA had the 1p/19q co-deletion (Table 1). The *IDH* mutation was significantly associated with increased OS ($P = 0.0064$) and PFS ($P = 0.0001$) for patients with AA based on the univariate analysis. *TP53* mutation was also correlated with increased PFS ($P = 0.013$), but *MGMT* promoter methylation showed no significant association with PFS or OS.

In primary GBM, our univariate analysis showed that neither *IDH* mutation, 1p/19q co-deletion, nor *TP53* mutation was associated with PFS or OS, but *MGMT* promoter methylation was significantly associated with increased OS ($P = 0.0043$) and PFS ($P = 0.0038$).

Discussion

Here we report that *IDH* mutation, which was tightly associated with 1p/19q co-deletion and *MGMT* promoter methylation, was common in grade 2 gliomas and also, but to a lesser extent, in grade 3 gliomas. Moreover, we found that *IDH* mutation would be an especially useful genetic marker for evaluating the malignancy of grade 3 gliomas that do not have a 1p/19q co-deletion and that these gliomas were predominantly AA.

The frequencies and patterns of *IDH* mutation in our glioma samples from Japanese patients were largely comparable to those in previous reports.[2–7] *IDH* mutation was found predominantly in grade 2 glioma, such as DA, OA, and OG. *IDH* mutation frequencies were lower in higher-grade gliomas, and less than 10% of GBM had an *IDH* mutation; however, nearly half of secondary GBM, which developed from malignant transformation of lower-grade glioma, had an *IDH* mutation. These observations supported the notion that the *IDH* mutation has a crucial role in the development of the majority of grade 2 gliomas. In grade 3 gliomas, the oligodendroglial tumors had higher frequency of *IDH* mutation than astrocytic tumors (OG 76% > DA 59%, $P = 0.18$; AOG 67% > AA 28%, $P < 0.05$; Pearson's chi-square-test). No *IDH* mutation was detected in any grade 1 glioma, PA or GGL; this observation indicated that these tumors had a different genetic etiology from that of grade 2 and 3 infiltrative astrocytic and oligodendroglial tumors. This observation also supported the usefulness of *IDH* mutations along with BRAF alterations for differential diagnosis of PA.[27] However, our results differed from two previous reports that detected *IDH1* mutation (8–38%) in GGL.[5,28] Further studies are needed to clarify the biological and clinical significance of *IDH1* mutation in GGL.

As reported previously,[23] *TP53* mutation and co-deletion of chromosomes 1p and 19q were frequent alterations in grade 2 and grade 3 gliomas. The 1p/19q co-deletions were mostly found in oligodendroglial lineage gliomas, whereas *TP53* mutations were more frequent in gliomas derived from the astrocytic lineage. *IDH* mutation is currently believed to precede 1p/19q LOH and *TP53* mutation during the early stage of gliomagenesis,[4,6] and consistent with this hypothesis, most of our grade 2 gliomas that had 1p/19q co-deletion or *TP53* mutations also harbored an *IDH* mutation. In one study, all the gliomas with deletions of the entire 1p and 19q arms carried an *IDH1* or *IDH2* mutation;[26] however, we found a few exceptions in which there was 1p/19q LOH, but no *IDH* mutation. These apparent exceptions might have been artifacts due to our imperfect methods for detecting the extent of 1p/19q LOH, specifically microsatellite analysis or MLPA; these methods do not effectively differentiate partial chromosomal loss from typical entire 1p/19q hemizygous deletion, which is generally found in OG harboring *IDH* mutation. It would be better to carefully evaluate the extent of 1p/19q LOH in such exceptional cases. *TP53* mutation was also

doi: 10.1111/j.1349-7006.2011.02175.x

associated with *IDH* mutation in DA. However, there was no association between *IDH* and *TP53* mutation in AA or primary GBM. This observation suggested that *TP53* mutation promoted tumor growth independently of *IDH* mutation, especially in higher grade gliomas. Most gliomas with an *IDH* mutation had either 1p/19q LOH or *TP53* mutation, further supporting the hypothesis that combinations of *IDH* mutation and subsequent genetic alteration are common pathways leading to low-grade glioma. However, there were also a few other *IDH*-mutated gliomas that had neither 1p/19q co-deletion nor *TP53* mutation. In these gliomas, the kind of alterations subsequent to *IDH* mutation that caused progenitor cells to give rise to low-grade glioma remains to be elucidated.

Methylation at the *MGMT* promoter was associated with *IDH* mutation, especially for low-grade gliomas. Some IDH enzymes with a mutation in the catalytic domain acquire a novel enzymatic activity[9,11] that causes accumulation of 2-HG, and 2-HG is known to inhibit enzymes such as 5-methylcytosine hydroxylases and histone demethylases. As a result, *IDH* mutations bring about genome-wide hypermethylation, which might lead to tumor initiation.[12,29] Reportedly, the majority of low-grade gliomas have hypermethylated CpG islands throughout the genome; this phenomenon is called the glioma CpG island methylator phenotype, and these tumors frequently harbor *IDH* mutation.[30–32] Therefore, frequent *MGMT* promoter methylation in *IDH*-mutated low-grade glioma was possibly simply a reflection of hypermethylation of a plethora of genes resulting from the methylator phenotype. In contrast, the majority of GBM had *MGMT* promoter hypermethylation without also having *IDH* mutation, indicating that *MGMT* promoter methylation occurs independent of *IDH*-related hypermethylation in most GBM. Probably because of such a background, the prognostic values of *MGMT* promoter methylation for *IDH*-mutated and *IDH*-wild-type gliomas are not equal. In GBM, *MGMT* promoter methylation is a predictive factor for the efficacy of temozolomide, which is a common alkylating agent used in the chemotherapeutic treatment of malignant glioma.[33,34] However, the predictive value of *MGMT* promoter methylation for chemosensitivity in grade 2 and grade 3 glioma is controversial.[19,35]

The prognostic significance of *IDH* mutation differed among WHO tumor grades. Unlike previous reports, *IDH* mutation was not associated with the PFS or OS of our GBM patients; however, this finding might result from insufficient numbers of GBM patients with *IDH* mutation. A methylated *MGMT* promoter, which reflects the sensitivity of a tumor to temozolomide, was associated with favorable PFS and OS for patients with GBM, further emphasizing the importance of detecting *MGMT* promoter methylation status in GBM.

Among patients with grade 2 gliomas, *IDH* mutation was also not associated with prognosis. Wild-type *TP53* and 1p/19q co-deletion were each associated with prolonged PFS, probably because these two genetic alterations were mutually exclusive and tumors with wild-type *TP53* likely have a 1p/19q co-deletion, which is a recognized favorable prognostic factor. The prognostic value and predictability of temozolomide efficacy associated with *IDH* mutation in low-grade gliomas has been controversial. Consistent with our results, Kim *et al.*[20] showed that *IDH1* and *IDH2* mutations are not prognostic in low-grade gliomas, but that *TP53* mutation is a significant prognostic indicator of shorter survival and 1p/19q loss is prognostic of longer survival. However, Sanson *et al.*[15] reported a different result, specifically that *IDH1* mutation is associated with a better outcome in grade 2 gliomas. Dubbink *et al.*[18] showed that *IDH* mutation is associated with better outcomes for relapsed astrocytomas previously treated with radiotherapy, but there was no relationship between *IDH* mutation and temozolomide responsiveness. Houillier *et al.*[19] showed that *IDH1* or *IDH2* mutations predict better prognosis of glioma treated with temozolomide, but they did not appear to influence the course of untreated low-grade glioma. Thus, the prognostic value of *IDH* mutation is different from that of 1p/19q co-deletion, which is prognostic as well as predictive for responsiveness to temozolomide in low-grade gliomas. These inconsistent results on the association between *IDH* mutation and survival in cases of low-grade gliomas might be caused by the variable numbers of OG and DA included in these studies. Almost all oligodendroglial tumors with 1p/19q co-deletion also have an *IDH* mutation;[26] therefore, many cases of OG with favorable prognoses may affect and confound measurements of survival rate in the whole group of low-grade gliomas with *IDH* mutations. To avoid the confounding influence of OG, we also focused on DA with wild-type *IDH*; these tumors generally have neither 1p/19q LOH nor *TP53*. However, they had outcomes comparable to those of DA with *IDH* mutation. This finding indicated that DA with wild-type *IDH* was not more malignant than DA with an *IDH* mutation. This observation differed from the observation that AA with wild-type *IDH* had markedly worse outcomes than AA with an *IDH* mutation (OS, $P = 0.0064$; PFS, $P = 0.0001$).

In contrast with grade 2 and 4 gliomas, the prognostic significance of *IDH* mutation was evident for grade 3 gliomas, and this finding was consistent with previous reports.[15,17,36] Almost all gliomas with 1p/19q co-deletion have an *IDH* mutation,[26] and anaplastic oligodendroglial tumors often harbor 1p/19q co-deletion; therefore, monitoring of *IDH* mutation might have more clinical significance for patients with grade 3 gliomas with intact 1p/19q, and these tumors are predominantly AA. In fact, as the histopathological differential diagnosis of AA from GBM or DA is often subjective and diagnoses frequently differ between pathologists,[23] a pathological diagnosis of AA may not always indicate sameness between gliomas and similar prognosis. However, accurate determination of the pathological group of a tumor is clinically critical for planning adjuvant therapy, such as radiation and chemotherapy. Therefore, genetic analyses, which may reflect causative origins of tumors, are expected to reveal biological traits with less inter-observer variation, as is the case of 1p/19q co-deletion in oligodendroglial tumors. Because *IDH* mutations have a defined role in gliomagenesis and indicate, to some extent, the nature of the original tumor cell, monitoring *IDH* mutational status may allow for accurate assignment of diagnosed AA to low-grade gliomas that frequently harbor *IDH* mutation or to primary GBM that usually have intact *IDH*. Therefore, we believe that monitoring *IDH* mutation in combination with 1p/19q co-deletion, which genetically differentiates oligodendroglial and astrocytic tumors, could be a useful genetic marker of prognostic value, especially for grade 3 glioma patients.

Acknowledgments

We appreciate the technical assistance of Reiko Matsuura (Department of Neurosurgery, University of Tokyo, Tokyo, Japan). This work was supported in part by a Grant-in-Aid for Scientific Research (C) (No. 20591706) to A.M. and a Grant-in-Aid for Young Scientists (B) (No. 22791334) to K.S. from the Japan Society for the Promotion of Science. A.M. was also supported by the Takeda Science Foundation.

Disclosure Statement

The authors have no conflicts of interest.

Abbreviations

2-HG	2-hydroxyglutarate
AA	anaplastic astrocytoma
AOA	anaplastic oligoastrocytoma
AOG	anaplastic oligodendroglioma

DA	diffuse astrocytoma
GBM	glioblastoma
GBMO	glioblastoma with oligodendroglioma component
GGL	ganglioglioma
IDH	isocitrate dehydrogenase
LOH	loss of heterozygosity
MLPA	multiplex ligation-dependent probe amplification
OA	oligoastrocytoma
OG	oligodendroglioma
OS	overall survival
PA	pilocytic astrocytoma
PFS	progression-free survival

References

1 Louis DN, Ohgaki H, Wiestler OD, Cavenee WK, eds. *WHO Classification of Tumours of the Central Nervous System*, 4th edn. Lyon: International Agency for Research on Cancer, 2007.
2 Parsons DW, Jones S, Zhang X *et al.* An Integrated Genomic Analysis of Human Glioblastoma Multiforme. *Science* 2008; **321**: 1807–12.
3 Balss J, Meyer J, Mueller W, Korshunov A, Hartmann C, Deimling A. Analysis of the *IDH1* codon 132 mutation in brain tumors. *Acta Neuropathol (Berl)* 2008; **116**: 597–602.
4 Ichimura K, Pearson DM, Kocialkowski S *et al. IDH1* mutations are present in the majority of common adult gliomas but rare in primary glioblastomas. *Neuro Oncol* 2009; **11**: 341–7.
5 Sonoda Y, Kumabe T, Nakamura T *et al.* Analysis of *IDH1* and *IDH2* mutations in Japanese glioma patients. *Cancer Sci* 2009; **100**: 1996–8.
6 Watanabe T, Nobusawa S, Kleihues P, Ohgaki H. *IDH1* Mutations Are Early Events in the Development of Astrocytomas and Oligodendrogliomas. *Am J Pathol* 2009; **174**: 1149–53.
7 Yan H, Parsons DW, Jin G *et al. IDH1* and *IDH2* mutations in gliomas. *N Engl J Med* 2009; **360**: 765–73.
8 Mardis ER, Ding L, Dooling DJ *et al.* Recurring mutations found by sequencing an acute myeloid leukemia genome. *N Engl J Med* 2009; **361**: 1058–66.
9 Ward PS, Patel J, Wise DR *et al.* The Common Feature of Leukemia-Associated IDH1 and IDH2 Mutations Is a Neomorphic Enzyme Activity Converting α-Ketoglutarate to 2-Hydroxyglutarate. *Cancer Cell* 2010; **17**: 225–34.
10 Bleeker FE, Lamba S, Leenstra S *et al. IDH1* mutations at residue p.R132 ($IDH1^{R132}$) occur frequently in high-grade gliomas but not in other solid tumors. *Hum Mutat* 2009; **30**: 7–11.
11 Dang L, White DW, Gross S *et al.* Cancer-associated IDH1 mutations produce 2-hydroxyglutarate. *Nature* 2009; **462**: 739–44.
12 Xu W, Yang H, Liu Y *et al.* Oncometabolite 2-Hydroxyglutarate Is a Competitive Inhibitor of α-Ketoglutarate-Dependent Dioxygenases. *Cancer Cell* 2011; **19**: 17–30.
13 Lesniak M, Jin G, Reitman ZJ *et al.* 2-Hydroxyglutarate Production, but Not Dominant Negative Function, Is Conferred by Glioma-Derived NADP+-Dependent Isocitrate Dehydrogenase Mutations. *PLoS ONE* 2011; **6**: e16812.
14 Nobusawa S, Watanabe T, Kleihues P, Ohgaki H. *IDH1* Mutations as Molecular Signature and Predictive Factor of Secondary Glioblastomas. *Clin Cancer Res* 2009; **15**: 6002–7.
15 Sanson M, Marie Y, Paris S *et al.* Isocitrate Dehydrogenase 1 Codon 132 Mutation Is an Important Prognostic Biomarker in Gliomas. *J Clin Oncol* 2009; **27**: 4150–4.
16 Van den Bent MJ, Dubbink HJ, Marie Y *et al. IDH1* and *IDH2* Mutations Are Prognostic but not Predictive for Outcome in Anaplastic Oligodendroglial Tumors: a Report of the European Organization for Research and Treatment of Cancer Brain Tumor Group. *Clin Cancer Res* 2010; **16**: 1597–604.
17 Shibahara I, Sonoda Y, Kanamori M *et al. IDH1/2* gene status defines the prognosis and molecular profiles in patients with grade III gliomas. *Int J Clin Oncol* 2011; DOI: 10.1007/s10147-011-0323-2 [Epub ahead of print].
18 Dubbink HJ, Taal W, Van Marion R *et al. IDH1* mutations in low-grade astrocytomas predict survival but not response to temozolomide. *Neurology* 2009; **73**: 1792–5.
19 Houillier C, Wang X, Kaloshi G *et al. IDH1* or *IDH2* mutations predict longer survival and response to temozolomide in low-grade gliomas. *Neurology* 2010; **75**: 1560–6.
20 Kim Y-H, Nobusawa S, Mittelbronn M *et al.* Molecular Classification of Low-Grade Diffuse Gliomas. *Am J Pathol* 2010; **177**: 2708–14.
21 Jha P, Suri V, Sharma V *et al. IDH1* mutations in gliomas: first series from a tertiary care centre in India with comprehensive review of literature. *Exp Mol Pathol* 2011; **91**: 385–93.
22 Qi SA, Yu L, Lu YT *et al. IDH* mutations occur frequently in Chinese glioma patients and predict longer survival but not response to concomitant chemoradiotherapy in anaplastic gliomas. *Oncol Rep* 2011; **26**: 1479–85.
23 Ueki K, Nishikawa R, Nakazato Y *et al.* Correlation of histology and molecular genetic analysis of 1p, 19q, 10q, *TP53*, *EGFR*, *CDK4*, and *CDKN2A* in 91 astrocytic and oligodendroglial tumors. *Clin Cancer Res* 2002; **8**: 196–201.
24 Mukasa A, Ueki K, Matsumoto S *et al.* Distinction in gene expression profiles of oligodendrogliomas with and without allelic loss of 1p. *Oncogene* 2002; **21**: 3961–8.
25 Esteller M, Hamilton SR, Burger PC, Baylin SB, Herman JG. Inactivation of the DNA repair gene O6-methylguanine-DNA methyltransferase by promoter hypermethylation is a common event in primary human neoplasia. *Cancer Res* 1999; **59**: 793–7.
26 Labussiere M, Idbaih A, Wang XW *et al.* All the 1p19q codeleted gliomas are mutated on *IDH1* or *IDH2*. *Neurology* 2010; **74**: 1886–90.
27 Korshunov A, Meyer J, Capper D *et al.* Combined molecular analysis of *BRAF* and *IDH1* distinguishes pilocytic astrocytoma from diffuse astrocytoma. *Acta Neuropathol* 2009; **118**: 401–5.
28 Horbinski C, Kofler J, Yeaney G *et al.* Isocitrate dehydrogenase 1 analysis differentiates gangliogliomas from infiltrative gliomas. *Brain Pathol* 2011; **21**: 564–74.
29 Figueroa ME, Abdel-Wahab O, Lu C *et al.* Leukemic IDH1 and IDH2 Mutations Result in a Hypermethylation Phenotype, Disrupt TET2 Function, and Impair Hematopoietic Differentiation. *Cancer Cell* 2010; **18**: 553–67.
30 Christensen BC, Smith AA, Zheng S *et al.* DNA Methylation, Isocitrate Dehydrogenase Mutation, and Survival in Glioma. *J Natl Cancer Inst* 2010; **103**: 143–53.
31 Laffaire J, Everhard S, Idbaih A *et al.* Methylation profiling identifies 2 groups of gliomas according to their tumorigenesis. *Neuro Oncol* 2010; **13**: 84–98.
32 Noushmehr H, Weisenberger DJ, Diefes K *et al.* Identification of a CpG Island Methylator Phenotype that Defines a Distinct Subgroup of Glioma. *Cancer Cell* 2010; **17**: 510–22.
33 Hegi ME, Diserens AC, Gorlia T *et al. MGMT* gene silencing and benefit from temozolomide in glioblastoma. *N Engl J Med* 2005; **352**: 997–1003.
34 Rivera AL, Pelloski CE, Gilbert MR *et al.* MGMT promoter methylation is predictive of response to radiotherapy and prognostic in the absence of adjuvant alkylating chemotherapy for glioblastoma. *Neuro Oncol* 2010; **12**: 116–21.
35 Van den Bent MJ, Dubbink HJ, Sanson M *et al. MGMT* promoter methylation is prognostic but not predictive for outcome to adjuvant PCV chemotherapy in anaplastic oligodendroglial tumors: a report from EORTC Brain Tumor Group Study 26951. *J Clin Oncol* 2009; **27**: 5881–6.
36 Hartmann C, Hentschel B, Wick W *et al.* Patients with *IDH1* wild type anaplastic astrocytomas exhibit worse prognosis than *IDH1*-mutated glioblastomas, and *IDH1* mutation status accounts for the unfavorable prognostic effect of higher age: implications for classification of gliomas. *Acta Neuropathol (Berl)* 2010; **120**: 707–18.

doi: 10.1111/j.1349-7006.2011.02175.x

Successful Treatment of Leptomeningeal Gliomatosis of Pilomyxoid Astrocytoma After Failed Frontline Chemotherapy

Mizuhiko Terasaki, MD, PhD, Eric Bouffet, MD,† Mitsuhide Maeda, MD, PhD,* Yasuo Sugita, MD, PhD,‡ Yutaka Sawamura, MD, PhD,§ and Motohiro Morioka, MD, PhD**

Introduction: Pilomyxoid astrocytoma (PMA) is a rare variant of pilocytic astrocytoma. Compared with pilocytic astrocytoma, PMA is more aggressive, has a higher rate of local recurrence, and often disseminates to the leptomeninges. Leptomeningeal gliomatosis is another rare but often intractable neoplasm. PMA presenting as leptomeningeal gliomatosis can be a therapeutic challenge, particularly in young children for whom many pediatric oncologists consider radiation therapy only as a back-up treatment. However, chemotherapy, usually considered a frontline treatment for low-grade tumors such as PMA, has little impact on leptomeningeal gliomatosis.

Case Report: We report on a 5-year-old boy with an approximately 2-month history of progressively worsening loss of vision. Radiographic studies with contrast revealed an enhanced mass within the optic nerve, an enhanced lesion in the leptomeninges, and diffusely scattered nonenhanced white matter lesions in the craniospinal axis. The patient was treated with a 10-week carboplatin and vincristine regimen without a biopsy. After completing induction and 1 maintenance cycle, however, the patient developed coma caused by hydrocephalus. External ventricular drainage was performed and a biopsy was taken through ventriculoscopy, revealing PMA. The patient was then treated with craniospinal irradiation and concomitant temozolomide, a regimen to which he had a complete response. Two years after initial presentation the patient was free of disease.

Conclusions: This report documents a rare, intractable tumor and provides evidence that radiation therapy, given as craniospinal irradiation, can be effective for leptomeningeal gliomatosis.

Key Words: gliomatosis, leptomeningeal, pilomyxoid astrocytoma

(*The Neurologist* 2012;18:32–35)

Pilomyxoid astrocytoma (PMA) is a rare glioma, histologically composed of compact, piloid cells, and a predominantly myxoid background.[1–3] The disease shares histopathologic similarities with pilocytic astrocytoma (PA), and early studies describe PMA as a manifestation of PA.[3] More recent reports consider PMA a separate entity, because it differs from PA in histology (eg, PMA lacks Rosenthal fibers), demonstrates more aggressive behavior (higher mortality and shorter disease-free survival), and tends to present in younger patients.[1,2] Some evidence suggests that the relationship between PMA and PA is closer, however, with the latter disease being, from a morphologic perspective, a rare "maturation" phenomenon of the former.[4] Although no standard of care has been established for PMA, the disease is often treated as a low-grade tumor with frontline therapy being based on morphology.[2]

PMA tends to disseminate to the leptomeninges more frequently than PA does.[5] However, a literature search revealed only 1 report that discussed leptomeningeal seeding from PMA in an adult.[5] That patient was initially treated with a combined regimen of radiotherapy and temozolomide (TMZ); however, disease recurred in the spinal area outside the radiation field. This case suggests that PMA can spread as leptomeningeal gliomatosis.

We report on a child with PMA presenting as leptomeningeal gliomatosis who failed to respond to frontline chemotherapy but had a good outcome on our treatment regimen of combined craniospinal irradiation (CSI) and TMZ.

CASE STUDY

A 5-year-old boy complained of progressive visual loss lasting nearly 2 months. Physical examination revealed no manifestations of neurofibromatosis type 1. Cranial magnetic resonance (MR) imaging showed a thick mass within the optic nerve and chiasm; the lesion was isointense on T1-weighted images and hyperintense on T2-weighted images. After contrast administration the lesion enhanced in association with diffuse leptomeningeal enhancement (Fig. 1A). Spinal MR imaging revealed diffuse enhancement of the spinal leptomeninx at all levels (Fig. 1B). Because these MR imaging findings were consistent with optic nerve and leptomeningeal dissemination of the tumor, we decided to proceed with frontline chemotherapy of carboplatin (CBDCA) and vincristine (VCR) without biopsy. The child accordingly received a 10-week induction regimen of CBDCA and VCR according to the schedule previously described by Packer et al.[6] CBDCA was administered at a dose of 175 mg/m^2 as an intravenous infusion on days 0, 7, 14, 21, 42, 49, 56, and 63. VCR was administered at a dose of 1.5 mg/m^2 as an intravenous bolus infusion on days 0, 7, 14, 21, 28, 35, 42, 49, 56, and 63.

Because MR images taken after induction chemotherapy indicated stable disease (defined as a decrease of <25% or an increase of <25% in measurable tumor area), the patient proceeded to maintenance chemotherapy consisting of CBDCA at a dose of 175 mg/m^2 as an intravenous infusion on days 0, 7, 14, and 21 and VCR at a dose of 1.5 mg/m^2 as an intravenous bolus infusion on days 0, 7, and 14 of each cycle, followed by a 2-week rest period. However, after the first maintenance cycle, the boy developed deep coma caused by hydrocephalus. An external ventricular drain was inserted to relieve pressure, and endoscopic biopsy was performed. After cerebrospinal fluid (CSF) drainage, the patient's orientation improved and he became more alert. Pathologic examination of the biopsy specimen and cytologic analysis of the collected CSF sample were consistent with a diagnosis of PMA (Figs. 2A, B). CSF showed pleocytosis and a high protein concentration of 70 mg/dL (normal 9 to 42 mg/dL). Monoclonal antibody staining to determine proliferating capacity of the biopsied sample, as indicated by the frequency of Ki-67-positive cells, was high at 20%.

After the fifth maintenance cycle, MR imaging showed a mixed response with shrinkage of the optic nerve lesion contrasting with

From the *Departments of Neurosurgery; ‡Pathology, Kurume University School of Medicine, Fukuoka; §Sawamura Neurology and Neurosurgery Clinica, Hokkaido, Japan; and †Department of Pediatrics, Hospital for Sick Children, Toronto, Ontario, Canada.

The authors declare no conflict of interest.

Reprints: Mizuhiko Terasaki, MD, PhD, Department of Neurosurgery, Kurume University School of Medicine, 67 Asahimachi, Kurume, Fukuoka 830-0011, Japan. E-mail: jintara@med.kurume-u.ac.jp.

ISSN: 1074-7931/12/1801-0032
DOI: 10.1097/NRL.0b013e31823d7a92